NASA Technical Memorandum 78483



# Calculated Rate Constants for the Reaction ClO + O → Cl + $O_2$ Between 220 and 1000 °K

Richard L. Jaffe

April 1978


National Aeronautics and
Space Administration

NASA Technical Memorandum 78483

# Calculated Rate Constants for the Reaction ClO + O → Cl + $O_2$ Between 220 and 1000 °K

Richard L. Jaffe, Ames Research Center, Moffett Field, California

NASA
National Aeronautics and
Space Administration

**Ames Research Center**
Moffett Field, California 94035

# Calculated rate constants for the reaction $ClO + O \rightarrow Cl + O_2$ between 220 and 1000 °K

Richard L. Jaffe*

NASA Ames Research Center

Moffett Field, California 94035

The results of classical trajectory calculations are presented for the reaction $ClO + O \rightarrow Cl + O_2$. This reaction is an important step in the chlorine-catalyzed destruction of ozone which is thought to occur in the stratosphere. Rate constants have been calculated for temperatures between 220 and 1000 °K. The calculated rate constant is $4.36 \times 10^{-11} \exp(-191/T)$ $cm^3$ $molecule^{-1}$ $s^{-1}$ and its value at 300 °K is $2.3 \pm 0.2 \times 10^{11}$ $cm^3$ $molecule^{-1}$ $s^{-1}$, about a factor of 2 lower than the recent experimental measurements. The calculated activation energy of 0.38 kcal/mole is in excellent agreement with the experimental value of 0.44 kcal/mole determined by Clyne and Nip and provides support for their measurements. The calculations were performed using both the quasi-classical and phase space trajectory sampling methods. The empirical potential energy surface used in the calculations was constructed to fit experimental data for ClO, $O_2$ and ClOO molecules. Other important features of this potential surface, such as the barrier to reaction, were varied systematically and calculations were performed for a range of conditions to determine the "best" theoretical rate constants. The present results demonstrate the utility of classical trajectory methods for determining activation energies and other kinetic data for important atmospheric reactions.

## I. INTRODUCTION

The potential threat of chlorine-catalyzed depletion of the stratospheric ozone layer has received considerable attention since Molina and Rowland[1,2] suggested that anthropogenic chlorofluorocarbons may provide a significant source of atomic chlorine in the stratosphere.[3] In fact, this proposal[1] has stimulated a tremendous research effort in aeronomy[4-7] and chemical kinetics.[8,9] Previously, a ClX cycle had been proposed as a possible sink for stratospheric ozone,[10-12] but no major sources of chlorine had been identified. Since that time calculations have indicated that the chlorofluorocarbons may cause serious depletion of the stratospheric ozone layer.[13]

The principal active chlorine species in the stratospheric ClX cycle are Cl and ClO. At high altitudes (40-50 km), the ozone depletion is a result of the cyclic process:

$$Cl + O_3 \rightarrow ClO + O_2 \qquad (R1)$$

$$ClO + O \rightarrow Cl + O_2 \ . \qquad (R2)$$

Since atomic oxygen and ozone are in equilibrium, the removal of either odd oxygen species is important. At lower altitudes, the concentration of atomic oxygen is low enough that the reaction (R2) is in competition with

$$ClO + NO \rightarrow Cl + NO_2 \qquad (R3)$$

which is the dominant process below 20 km. Other ClO reactions,

$$ClO + CO \rightarrow Cl + CO_2 \qquad (R4)$$

$$ClO \xrightarrow{h\nu} Cl + O \qquad (R5)$$

$$ClO + ClO \rightarrow \text{products} \qquad (R6)$$

$$ClO + O_3 \rightarrow \text{products} \ , \qquad (R7)$$

are possible, but less important at stratospheric conditions owing to lower rate constants or reactant concentrations.

Clearly the chemistry of ClO, and particularly the ClO + O reaction, plays an important role in the overall ClX cycle. An accurate determination of the relative amounts of ClO consumed by each of these processes requires knowledge of all the rate constants for reactions (R2) - (R7) at the ambient temperatures, which range from 210 to 270 °K for the altitudes of interest (20-60 km).[2,6] Unfortunately, complete reaction rate data are not available for these reactions. The rate constant for (R2) has been measured in several laboratories at 300 °K using ultraviolet spectroscopy,[14,15] mass spectrometry,[16,17] and atomic resonance fluorescence detection methods.[17] The most widely accepted value[17] for that rate constant is $(5.3 \pm 0.8) \times 10^{-11}$ $cm^3$ $molecule^{-1}s^{-1}$ with the earlier workers[14-16] giving values between 1 and $2 \times 10^{-11}$. Two very recent measurements[19,20] have confirmed the work of Bemand, Clyne, and Watson[17] yielding rate constants of $(5.2 \pm 1.6) \times 10^{-11}$ and $(4.4 \pm 0.9) \times 10^{-11}$ $cm^3$ $molecule^{-1}s^{-1}$, respectively, at 300 °K. These studies[18,19] also provide the first experimental determinations of the rate constants between 220 and 426 °K. While the observed temperature dependences are both small, the data are not in agreement since one study[19] yields a negative activation energy. In addition, Park[20] has measured the rate constant for (R2) between 1000 and 1500 °K in shock tube experiments and reports an averaged result of $(7 \pm 1.5) \times 10^{-11}$ $cm^3$ $mole^{-1}s^{-1}$ at 1250 °K. Consequently, the variation of the experimental data between 300 °K[17-19] and 1250 °K[20] is extremely small. According to collision theory, the rate constant for reactions with zero activation energy should still exhibit a temperature dependence.[21,22] However, the observed temperature dependence[17-20] is slightly less than the minimum expected on these grounds. In addition, the relatively

large uncertainties in the measured rate constants make it difficult for one to extrapolate the rate constant data to lower temperatures with confidence.

Reaction (R3) has been studied by Clyne and Watson[23] and Zahniser and Kaufman[19] who report rate constants of $(1.7 \pm 0.2) \times 10^{-11}$ and $(2.3 \pm 0.8) \times 10^{-11}$ $cm^3$ $molecule^{-1}s^{-1}$ at 300 °K, respectively. The amount of ozone depletion predicted by the stratospheric models is very sensitive to the ratio $K_2/K_3$.[13] Thus, it is of extreme importance that the temperature dependence of these rate constants be accurately known. The rate constants for (R4), (R6), and (R7) have been measured at 300 °K and are 3-5 orders of magnitude lower than the above.[23,24] Photodissociation cross sections for ClO have been determined by Johnston et al.[25] between 2250 and 2800 Å and predissociation is known to occur at longer wavelengths.[26,27] The ground state absorption probability is too small for photodissociation to contribute to the overall ClO chemistry in the stratosphere except at very high altitudes.[3,11] Predissociation is more rapid but it is still not important at altitudes between 20 and 50 km.[28]

The present paper describes classical trajectory calculations of ClO + O collisions which have been performed to determine the reaction kinetics and dynamics of (R2). Previous studies on the $H_2 + D$[29] and $H_2 + F$[30-32] exchange reactions, among others, have shown that classical trajectory methods can be used to compute accurate rate constants, reaction cross sections, product vibrational and rotational energy distributions, etc. One requirement of these calculations is that the potential energy surface for the particular reaction system must be known. However, for most reactions of importance to stratospheric chemistry, this is not the case. In the present work, an attempt is made to construct a reasonable potential energy surface for (R2)

based on experimental spectroscopic and thermodynamic data that are suitable for use in classical trajectory calculations. The development of reliable methods for constructing potential energy surfaces will permit the extension of classical trajectory calculations to a wide range of important chemical reactions.

Part II of this paper describes certain physical properties of the Cl-O-O system based on the available experimental data. These properties are used as a guide in the construction of a family of empirical potential energy surfaces which are presented in Part III. The set of surfaces spans a reasonable range of topographies for $ClO_2$, and should bracket the true potential surface which is not known. In Part IV, we give a brief description of the classical trajectory method used in this work. Part V contains a discussion of the results of the reaction cross section and rate constant calculations performed for reaction (R2) for the temperature range 220-1000 °K. The calculated rate constants are compared with the experimental measurements and used to describe the temperature dependence of this reaction. Finally, in Part VI we summarize these calculations and briefly discuss the implications of the present study on the chemistry of ClO in the stratosphere.

## II. PHYSICAL CHARACTERISTICS OF THE Cl-O-O SYSTEM

In this section we summarize those properties of the Cl-O-O system which are used in the construction of the potential energy surface for reaction (R2) described in section III. First the reactant (ClO + O) and product (Cl + $O_2$) limits are discussed and then the properties of the stable triatomic species are presented along with the adiabatic correlations between the triatomic molecules and the atom-diatom limits.

A. The ClO + O Limit

The ground state of the ClO molecule $X^2\Pi_{3/2}$ is known to dissociate to ground state atoms ($Cl^2P_{3/2}$ and $O^3P_2$).[26,33-35] The dissociation energy (63.427 ± 0.009 kcal/mole) has been measured by Coxon and Ramsey[27b] and by Durie and Ramsay.[26] Until recently, the detailed shape of the ground state potential curve was not well known since progressions had been observed only for $v \leq 2$ in absorption[27b,35] and for $5 \leq v \leq 9$ in emission.[27a] However, accurate ab initio MCSCF+CI potential curves have been obtained for the $X^2\Pi$ and $A^2\Pi$ states of ClO by Arnold, Whiting, and Langhoff.[36] Their calculated ground state dissociation energy is within 2 kcal/mole of the above experimental value. At 300 °K, only 1.8% of the $X^2\Pi$ ClO molecules is in excited vibrational states (this decreases to 0.2% at 220 °K). However, the rotational spacings[33] are small and a broad thermal rotational distribution exists, even at 220 °K. The peak at 220 °K occurs for $J \cong 12$, and significant populations exist for $J \geq 30$ (1.77%). These data for ClO are summarized in Table I, based on Refs. 26, 33-35. Basco and Morse[35] have determined the $^2\Pi_{3/2} \rightarrow {}^2\Pi_{1/2}$ spin orbit coupling constant to be 318 $cm^{-1}$ ($\Delta E$ = 1.364 kcal/mole), resulting in 90.8% of all ClO being in the $X^2\Pi_{3/2}$ state at 300 °K (95.8% at 220 °K). Thus, a thermal ensemble of ClO at stratospheric temperatures consists mainly of molecules with excited rotational levels within the ground vibrational and electronic state manifolds.

At low temperatures only ground state oxygen atoms ($^3P_g$) exist in thermal systems. In the stratosphere less than 0.1% of the oxygen atoms is electronically excited and these are considered to be separate chemical species in most treatments of stratospheric chemistry. There are three fine structure states for O ($^3P_g$):[33,38] $^3P_2$, the ground state, $^3P_1$ (0.453 kcal/mole above

the ground state) and the $^3P_0$ state (0.648 kcal/mole higher in energy than $^3P_2$). At 220 °K, 79.5% of a thermal sample will be in the ground fine structure state.

There are six possible fine structure-state combinations for ClO ($^2\Pi$) + O ($^3P$) collisions and their relative thermal collision frequencies are given in Table II. At temperatures up to 1000 °K the ground state ($^2\Pi_{3/2}$ + $^3P_2$) is by far the most probable. However, the ($^2\Pi_{3/2}$ + $^3P_1$) and ($^2\Pi_{3/2}$ + $^3P_0$) combinations also occur with appreciable probability in low-temperature thermal collisions.

B. The $O_2$ + Cl Limit

In contrast to ClO, the lower electronic states of $O_2$ have been extremely well characterized. Three of these states are energetically accessible as products of reaction (R2): $^3\Sigma_g^-$, $^1\Delta_g$ ($T_e$ = 22.64 kcal/mole) and $^1\Sigma_g^+$ ($T_e$ = 37.73 kcal/mole).[34] The ground state reaction is highly exothermic:[33]

$$ClO(^2\Pi) + O(^3P_g) \rightarrow Cl(^2P_u) + O_2(^3\Sigma_g^- v' \leq 13), \quad \Delta H^\circ_{f_{298}} = -54.76 \text{ kcal/mole} , \quad \text{(R2a)}$$

as are the reactions which form the first two excited states of $O_2$,

$$ClO(^2\Pi) + O(^3P_g) \rightarrow Cl(^2P_u) + O_2(^1\Delta_g v' \leq 7), \quad \Delta H^\circ_{f_{298}} = -32.26 \text{ kcal/mole} , \quad \text{(R2b)}$$

$$ClO(^2\Pi) + O(^3P_g) \rightarrow Cl(^2P_u) + O_2(^1\Sigma_g^+ v' \leq 4), \quad \Delta H^\circ_{f_{298}} = -17.29 \text{ kcal/mole} . \quad \text{(R2c)}$$

However, there is presently no positive experimental evidence for singlet oxygen formation (i.e., reaction (R2b) or (R2c)).

Lipscomb, Norrish, and Thrush[39] and Basco and coworkers[15,40,41] have observed vibrationally excited $O_2$ produced by reaction (R2a). They found that the v' = 2 to v' = 7 levels (primed quantum numbers refer to product molecules and unprimed quantum numbers refer to reactants) were equally populated,

the ground state) and the $^3P_0$ state (0.648 kcal/mole higher in energy than $^3P_2$). At 220 °K, 79.5% of a thermal sample will be in the ground fine structure state.

There are six possible fine structure-state combinations for ClO ($^2\Pi$) + O ($^3P$) collisions and their relative thermal collision frequencies are given in Table II. At temperatures up to 1000 °K the ground state ($^2\Pi_{3/2}$ + $^3P_2$) is by far the most probable. However, the ($^2\Pi_{3/2}$ + $^3P_1$) and ($^2\Pi_{3/2}$ + $^3P_0$) combinations also occur with appreciable probability in low-temperature thermal collisions.

B. The $O_2$ + Cl Limit

In contrast to ClO, the lower electronic states of $O_2$ have been extremely well characterized. Three of these states are energetically accessible as products of reaction (R2): $^3\Sigma_g^-$, $^1\Delta_g$ ($T_e$ = 22.64 kcal/mole) and $^1\Sigma_g^+$ ($T_e$ = 37.73 kcal/mole).[34] The ground state reaction is highly exothermic:[33]

$$ClO(^2\Pi) + O(^3P_g) \rightarrow Cl(^2P_u) + O_2(^3\Sigma_g^- v' \leq 13), \quad \Delta H^\circ_{f_{298}} = -54.76 \text{ kcal/mole} , \quad \text{(R2a)}$$

as are the reactions which form the first two excited states of $O_2$,

$$ClO(^2\Pi) + O(^3P_g) \rightarrow Cl(^2P_u) + O_2(^1\Delta_g v' \leq 7), \quad \Delta H^\circ_{f_{298}} = -32.26 \text{ kcal/mole} , \quad \text{(R2b)}$$

$$ClO(^2\Pi) + O(^3P_g) \rightarrow Cl(^2P_u) + O_2(^1\Sigma_g^+ v' \leq 4), \quad \Delta H^\circ_{f_{298}} = -17.29 \text{ kcal/mole} . \quad \text{(R2c)}$$

However, there is presently no positive experimental evidence for singlet oxygen formation (i.e., reaction (R2b) or (R2c)).

Lipscomb, Norrish, and Thrush[39] and Basco and coworkers[15,40,41] have observed vibrationally excited $O_2$ produced by reaction (R2a). They found that the $v' = 2$ to $v' = 7$ levels (primed quantum numbers refer to product molecules and unprimed quantum numbers refer to reactants) were equally populated,

and that the population gradually increased from the $v' = 8$ to $v' = 13$ levels. Small populations were observed for $v' = 0,14$ and there was a large rate of formation for $O_2$ $v' = 1$. They found that approximately 45% of the heat of reaction was channeled into $O_2$ vibration.[41] Even though large uncertainties exist in the measured $O_2$ vibrational distribution, these data demonstrate that the major products of reaction (R2) are vibrationally excited $O_2$ $^3\Sigma_g^-$ and Cl $^2P_u$. Based on these measurements[41] and the work of Polanyi and coworkers,[42,43] who have correlated the nature of the "energy release" on potential energy surfaces with product vibrational energy distributions, one can conclude that reaction (R2a) proceeds along a predominately "attractive and mixed" potential energy surface.

The splittings between the fine-structure states of $^3\Sigma_g^-$ $O_2$ are sufficiently small ($\sim$2 $cm^{-1}$) to be considered zero. Some of the important physical constants for $O_2$ are listed in Table I. The ground state of the chlorine atom has $^2P_u$ symmetry with a spin orbit splitting between the $^2P_{3/2}$ and $^2P_{1/2}$ states of 2.523 kcal/mole.[38] There is no experimental evidence for preferential formation of one of the fine structure states in reaction (R2). At low temperatures, no other electronic states of Cl can be formed in this reaction.

## C. Triatomic $ClO_2$

There are two distinct isomers of $ClO_2$. One (OClO) is a chemically stable free radical at room temperature whose ground state has $C_{2v}$ symmetry. The other, a peroxy-like radical (ClOO) of $C_s$ symmetry, is highly reactive and has been observed only at low temperatures. ClO + O collisions must pass through intermediate geometries resembling the structure ClOO in order to form Cl + $O_2$ products.

The existence of an unstable ClOO species was first proposed by Benson and Buss[44] in order to account for certain observations of chlorine chain reactions. They estimated that ClOO has a lower total energy than OClO and that its high reactivity is due to a very weak Cl-O bond. Confirmation of their hypothesis has come from matrix IR[45] and ESR[46] experiments. In the former, Arkell and Schwager have determined the equilibrium geometry and force constants. They found ClOO to have a bond angle of 110°, a weak and elongated Cl-O bond, and an O-O bond similar to that found in $O_2$. Restricted Hartree-Fock calculations for ClOO have identified the symmetries of the two lowest electronic states as $^2A''$ and $^2A'$ ($T_e < 1$ eV).[47,48] Johnston and coworkers,[25] Wagman and Garvin,[49] and, most recently, Clyne, McKenney, and Watson[24] have revised the values for the heat of formation of ClO and ClOO. The most recent estimates of the Cl-O and O-O bond energies are 7.7 and 62.7 kcal/mole, respectively, and ClOO is thermodynamically more stable than OClO by 3.1 kcal/mole. Some of the physical constants for the electronic ground states of ClOO and OClO are listed in Table III. Figure 1 is a schematic energy diagram of the low-lying states of $ClO_2$.

D. Adiabatic Electronic State Correlations

In order to connect the atom-diatomic and triatomic regions of the $ClO_2$ potential surface, one must consider the adiabatic electronic state correlations under the appropriate symmetry restrictions. Shuler[50] outlined the basic method for determining the symmetries of atomic and diatomic ($C_{\infty v}$ and $D_{\infty h}$) fragments under lower point groups (e.g., $C_s$ or $C_{2v}$ for nonlinear triatomic molecules). For the present case, 6 doublet and 6 quartet states arise from the combination of a $^3P_g$ atom with a $^2\Pi$ diatomic. The doublet surfaces are the only ones of importance in the present work, since the quartet surfaces

correlate with high energy states of ClOO.[48] Of the 6 possible states in $C_s$ symmetry, 3 are A' and 3 are A". The first $^2A"$ state correlates with the ClOO ground electronic state and the first $^2A'$ state correlates with the low lying excited state of ClOO discussed above. The energies of the 4 other states of ClOO that dissociate to ground state ClO + O are not known. Similarly, $O_2(^3\Sigma_g^-) + Cl(^2P_u)$ correlates to $^2A' + 2\ ^2A"$ (and 3 quartets). The resulting correlation between reactants, intermediates and products for (R2) is shown in Fig. 2. Only the $^3\Sigma_g^-$ and $^1\Delta_g$ oxygen products correlate to ground state reactants in $C_s$ symmetry.[50] Since the $1\ ^2A'$ and $2\ ^2A"$ states of ClOO correlate to the ground state of $Cl + O_2$ (only ~8 kcal/mole above $1\ ^2A"$), they are most likely not bound.

Fine structure effects can also be estimated by the use of extended point groups[51,52] to combine the orbital and spin symmetries. All polyatomic states ($^2A'$ and $^2A"$) become $^2E_{1/2}$ symmetry and a one-to-one correspondence between reactant and product fine structure states can be made by invoking the non-crossing rule[53] (see Fig. 2). The $(^2\Pi_{3/2} + {}^3P_2)$, $(^2\Pi_{3/2} + {}^3P_1)$, and $(^2\Pi_{1/2} + {}^3P_2)$ reactant combinations are most probable in thermal systems. The first two correlate with $(^2P_{3/2} + {}^3\Sigma_g^-)$ products through the $1\ ^2A"$ and $1\ ^2A'$ states of ClOO and the third correlates with $(^2P_{3/2} + {}^1\Delta_g)$ products. Of course these correlations hold only within the adiabatic representation. Nonadiabatic effects, such as surface hopping or electronic transitions, could lead to the formation of $^1\Sigma_g^+$ $O_2$.[54]

These thermodynamic and spectroscopic data combined with the electronic correlations provide a good qualitative picture of the Cl-O-O system. Much of this information is used in the construction of a set of empirical potential energy surfaces which is described in the next section.

## III. THE POTENTIAL ENERGY SURFACE

Most calculations of collisional phenomena require as input the potential energy of the system for a large volume of configuration space. Since accurate ab initio calculations of the potential energy are not usually available, empirical and semiempirical valence-bond methods (such as LEPS[42,55]) have been devised to represent potential surfaces. In the present case, an accurate ab initio potential surface is unavailable and the LEPS formulation is not suitable, since LEPS potential surfaces always favor collinear triatomic geometries. Empirical angular dependencies have been artificially introduced into the LEPS framework by either supplying an additional angle dependent term[56] or by modifying the standard repulsive potentials for the diatomic fragments.[57] However, these approaches do not yield satisfactory results for ClOO. In this section an empirical model for the ClOO potential energy surface is described based on the physical properties of the constituent species presented in Section II. The underlying rationale employed here should be generally applicable to the construction of potential surfaces for other chemical systems for which only limited experimental and/or theoretical data exist.

The potential energy surface for the ground state of $ClO_2$ has a deep well corresponding to the ClOO equilibrium geometry and troughs corresponding to separated atom-diatom geometries.[58] For reaction (R2) to occur, the oxygen atom must impinge on the oxygen end of the ClO molecule. The reaction coordinate for process (R2a) (i.e., the minimum energy path connecting separated ClO + O and $O_2$ + Cl geometries) must traverse the stable ClOO region of configuration space and the favored direction of approach for the colliding reactant species will be highly nonlinear (the Cl-O-O angle would be

approximately 110°). For the present study, the ground electronic state potential surface has been divided into 5 regions, as shown in Fig. 3: two separated atom-diatom regions for ClO + O and Cl + $O_2$, labeled I and V, respectively; a triatomic region for ClOO (III) and transition regions between the atom-diatom and triatomic configurations (II and IV). Mathematical expressions are given for the potential energy in regions I, III, and V and an interpolation scheme is presented to combine these formulae in the transition regions.

In the separated atom-diatom regions (I and V), the only contribution to the potential energy arises from the diatomic potential curve. For computational convenience, Morse functions ($V_M$) are used to represent the $^2\Pi_{3/2}$ ClO and $^3\Sigma_g^-$ $O_2$ diatomic molecules. The potential curves are constructed from the experimental well depth ($D_e$), equilibrium bond length ($R_e$) and vibrational constant ($\omega_e$) according to:[37]

$$V_M(R) = D_e\left\{1 - e^{-\beta(R-R_e)}\right\}^2 , \qquad \text{(III-1)}$$

where the parameter $\beta$ is given by

$$\beta = \left\{\frac{2\pi^2 c\mu}{D_e h}\right\}^{1/2} \omega_e . \qquad \text{(III-2)}$$

h, c, and $\mu$ are Planck's constant, the speed of light and the diatomic molecule reduced mass, respectively. Morse potentials are generally accurate near $R_e$ but they can deviate considerably from the exact potential curves at other internuclear separations. The calculations of Arnold, Whiting, and Langhoff[36] indicate that the true ClO potential curve rises more steeply at large R. However, only very low vibrational levels of ClO are populated under the conditions of the present study, and the fitted potential curve is expected to be adequate. On the other hand, the Morse function for $O_2$ exhibits a potential

well that is considerably narrower than the RKR curve.[59] In order to properly describe the reaction dynamics, the empirical potential surface should accurately reproduce the O-O interaction within the range of vibrational levels that might be populated by reaction (R2a) (1.00 Å $\leq$ R $\leq$ 1.62 Å for v' $\leq$ 14). A better fit (within 0.04 Å) to the RKR curve in this range is obtained by setting $\beta$ equal to 70% of the value given in Eq. (III-2).

The triatomic potential region III is represented by Morse functions for the Cl-O and O-O separations ($R_{ClO}$ and $R_{OO}$, respectively) and a double minimum "harmonic" potential for the Cl-O-O bond angle ($\alpha$). The Morse parameters are determined from the experimental force constants (f)[45] according to[37]

$$\beta = \{f/2D_e\}^{1/2} \ . \qquad \text{(III-3)}$$

For a nonlinear triatomic molecule the bending potential has a maximum at $\alpha = 180°$ (the so-called inversion barrier) and two minima at the equilibrium bond angles $\alpha_e$ and $(2\pi-\alpha_e)$. One expression for such a bending potential is

$$Y = AX^2 + \frac{B}{C + X^2} + D \ , \qquad \text{(III-4)}$$

where $X = \alpha - \pi$. This function has a maximum at $X = 0$ and minima at

$$X = \pm X_o = \pm\{-C + \sqrt{B/A}\}^{1/2} \ . \qquad \text{(III-5)}$$

The four parameters in Eq. (III-4) can be determined from $\alpha_e$, the bending force constant $f_B$, the height of the inversion barrier $E^*$, and the requirement that $Y(X_o) = 0$. The derivation is given in the Appendix.

In summary, the potential energy in each of the above three regions is given by:

$$V_I = V_M(R_{ClO}) \ , \qquad \text{(III-6a)}$$

$$V_{III} = V_{M'}(R_{ClO}) + V_{M'}(R_{OO}) + Y(\alpha) + V_{REF1} \qquad \text{(III-6b)}$$

and

$$V_V = V_M(R_{OO}) + V_{REF2} \quad , \tag{III-6c}$$

where $V_M$ and $V_{M'}$ symbolize Morse potentials parameterized for the diatomic and triatomic systems, respectively. $V_{REF1}$ and $V_{REF2}$ are the constants required to give the three potentials the common reference point as shown in Fig. 1 (separated reactants with ClO at $R_e$). For this case $V_{REF1}$ = -63.59 kcal/mole and $V_{REF2}$ = -55.83 kcal/mole.

The transition regions are defined by 2.2 Å $\leq R_{OO} <$ 3.0 Å for $V_{II}$ and 3.1 Å $\leq R_{Cl\text{-}OO} <$ 3.7 Å for $V_{IV}$, where $R_{Cl\text{-}OO}$ is the distance between Cl and the center-of-mass of the O-O fragment. The potential energy in these regions is constructed by interpolating between the triatomic and atom-diatom potentials. The interpolation is controlled by a "hyperbolic tangent-like function":

$$W(x) = \frac{\lambda(x - \rho)}{\lambda^2 + (x - \rho)^2} + \frac{1}{2} \quad , \quad |x - \rho| \leq \lambda \quad , \tag{III-7}$$

which switches between the two forms of the potential energy. x is $R_{OO}$ in region II and $R_{Cl\text{-}OO}$ in region IV. $\rho$ and $\lambda$ are parameters which fix the location of the center of the interpolation region and its width, respectively. W varies between 0 and 1 and $dW/dx = 0$ at $x = \rho \pm \lambda$. While this form of interpolation is continuous, it can introduce spurious local extrema into the potential energy surface. To prevent this, an extra term,

$$V_{PERT} = 4V_p W(x)[1 - W(x)] \quad , \tag{III-8}$$

has been added in each transition region to smooth the potential surface. The use of $V_{PERT}$ also permits the placement of adjustable barriers in the entrance and exit channels of the potential surface. For $V_{IV}$, $V_p$ = 0.5 kcal/mole for the zero barrier case when $\alpha = \alpha_e$ (the only one used)

and for $V_{II}$, $V_p$ = 3.0, 2.5, and 2.0 kcal/mole for $E_{BARR}$ = 0 (no barrier), 0.5 and 1.0 kcal/mole, respectively, when $\alpha = \alpha_e$.

The entire interpolation scheme is shown in Fig. 3 and summarized below. The potential energy function is first partitioned into two parts $V_A = V_I$ and

$$V_B = V_{III} , \quad R_{Cl-OO} < 3.1\text{Å} ; \tag{III-9a}$$

$$V_B = [1 - W(R_{Cl-OO})]V_{III} + W(R_{Cl-OO})V_V + V_{PERT}, \quad 3.1\text{Å} \leq R_{Cl-OO} < 3.7\text{Å} ; \tag{III-9b}$$

$$V_B = V_V , \quad R_{Cl-OO} \geq 3.7\text{Å} . \tag{III-9c}$$

Then $V_A$ and $V_B$ are connected by a similar interpolation to complete the construction of the potential surface:

$$V = V_B , \quad R_{OO} < 2.2\text{Å} ; \tag{III-10a}$$

$$V = W(R_{OO})V_A + [1 - W(R_{OO})]V_B + V_{PERT} , \quad 2.2\text{Å} \leq R_{OO} < 3.0\text{Å} ; \tag{III-10b}$$

$$V = V_A , \quad R_{OO} \geq 3.0\text{Å} . \tag{III-10c}$$

Equations (III-10b) and (III-9b) represent the potential in the transition regions $V_{II}$ and $V_{IV}$, respectively. Contour plots of the resulting potential surfaces for $\alpha$ = 90, 110, and 130° are shown in Fig. 4. The parameters used in the calculation of the potential energy are given in Table IV.

The empirical potential energy function described above should provide a good description of the actual potential surface in regions I, III, and V. A qualitative assessment of this potential can be made in terms of the nature of the energy release by using the reaction coordinate criterion of Polanyi and coworkers.[42] The formation of ClOO from ClO + O involves only mixed energy release since $R_{OO}$ decreases and $R_{ClO}$ increases as ClO and O approach. Likewise, the formation of ClOO from Cl + $O_2$ involves attractive energy release as the O-O bond length remains nearly constant during this process. Overall, the potential surface for reaction (R2) is classified as "mixed" and one

would expect a high degree of vibrational excitation in the products,[42,43] in agreement with experiment.[41]

While this potential energy surface seems to be very reasonable for reaction (R2a), the calculated reactior cross sections and rate constants will be most sensitive to the topography oi the potential surface in transition region II which is largely unknown. Topographical features like the height of the energy barrier, the O-O separation at the onset of ClO-O attraction in ClO + O collisions and the variation of the potential with $\alpha$ near the energy barrier will control the fraction of collisions which reach geometries corresponding to transient ClOO complexes and continue to products. Reasonable estimates based on experimental observations or a range of values have been used for these quantities in constructing the potential surfaces. It is hoped that future ab initio calculations of the potential energies will identify which of these choices is most reasonable. The magnitude of the energy barrier has been varied between 0 and 1.0 kcal/mole through the choice of $V_p$. The onset of the O-O attraction is governed in part by the shape of the O-O Morse potential in $V_{III}$ and by the location of the transition region II. The potential surface parameters given in Table IV result in an O-O attraction of 1 kcal/mole at $R_{OO} = 2.5$ Å for the zero-barrier surface. Great uncertainty lies in the selection of the rate of attenuation of the bending potential $Y(\alpha)$ as $R_{OO}$ and $R_{ClO}$ are increased. In the above formulation, the variation of the potential energy with $\alpha$ in region II is given by

$$V_\alpha = [1 - W(R_{OO})]Y(\alpha) \ . \qquad \text{(III-11)}$$

The magnitude of $V_\alpha$ at a particular value of $R_{OO}$ can be varied through the choice of boundaries for that transition region or through the choice $f_B$ and $E^*$. It must be noted that the latter affects the accuracy of the potential

in region III and could result in erroneous product angular and energy distributions.

## IV. CLASSICAL TRAJECTORY CALCULATIONS

The trajectory of a reactive collision corresponds to a unique path in phase space, proceeding from some reactant configuration to some product configuration. For electronically adiabatic collisions this path can usually be determined from the laws of classical mechanics,[60] provided that the potential energy surface is known. The classical motion of a system of $\mathcal{N}$ atoms is described by $6\mathcal{N}$ coupled first-order differential equations,

$$\frac{dQ_j}{dt} = \frac{\partial \mathcal{H}}{\partial P_j} , \qquad \text{(IV-1a)}$$

$$\frac{dP_j}{dt} = - \frac{\partial \mathcal{H}}{\partial Q_j} , \quad j = 1, 2, \ldots 3\mathcal{N} . \qquad \text{(IV-1b)}$$

The $Q_j$ and $P_j$ are the $3\mathcal{N}$ coordinates and conjugate momenta, respectively, needed to describe the system and $\mathcal{H}$ is the classical Hamiltonian (sum of kinetic and potential energies). This Hamiltonian, relative to the center-of-mass, is given by:

$$\mathcal{H} = \frac{1}{2\mu_{BC}} \sum_{j=1}^{3} P_j^2 + \frac{1}{2\mu_{A-BC}} \sum_{j=4}^{6} P_j^2 + V(Q_1, Q_2, \ldots, Q_6) , \qquad \text{(IV-2)}$$

for a triatomic system, A + BC. The coordinates $(Q_1, Q_2, Q_3)$ are the Cartesian components of the vector connecting atoms B and C and $(Q_4, Q_5, Q_6)$ are the components of the vector between atom A and the center-of-mass of BC. $\mu_{BC}$ and $\mu_{A-BC}$ are the reduced masses of atoms B and C and of atom A with diatomic BC, respectively. For $\mathcal{N} \geq 3$, numerical integration methods must be used to compute the trajectories.

In the present work a modified version of Muckerman's quasiclassical trajectory code[61] was used. This computer program contains an extremely accurate numerical integrator (11th order predictor – 11th order corrector) which is required to prevent the accumulation of truncation errors[62] when long-lived trajectories are computed. Individual classical trajectories are subject to the constraints of conservation of total energy $E_{TOTAL}$ and angular momentum L which are used to provide internal checks on the accuracy of the numerical integration. In the present work the changes in $E_{TOTAL}$ and L were typically less than one part in $10^5$ from the start to the finish of a trajectory. In addition, back integration of selected trajectories to return the initial coordinates constituted another check of the computational procedure.

Microanonical or canonical ensembles of colliding atoms and molecules can be simulated by calculating large numbers of trajectories with initial values for $Q_j$ and $P_j$ randomly selected from suitable distributions. There are several well-defined methods for selecting these initial conditions. Two of these, denoted the quasiclassical trajectory (QCT) and phase space trajectory (PST) sampling methods, have been used in the present work and are described briefly below.

A. Quasiclassical Trajectory Sampling Method

In the standard QCT sampling method the initial conditions are chosen to correspond to separated reactants with some relative momentum towards each other. The reactants are initially given classical vibration and rotation energies that correspond to quantum states of the isolated molecules. As Eqs. (IV-1) are numerically integrated, the species will first approach each other and then separate as products or the original reactants. The

quasiclassical trajectory sampling method (QCT) has been discussed in detail by Karplus, Porter, and Sharma[29] and in a recent review by Porter.[63]

The initial values of the coordinates $Q_i^\circ$ for the atom A and diatomic molecule BC in the (v,J) state are illustrated in Fig. 5. The three atoms lie in the X-Y plane of an arbitrary space-fixed coordinate system with $R_{BC}$ equal to one of the vibrational turning points of the (v,J) state and the angle of orientation, $\xi$, of BC randomly selected from a uniform distribution. Atom A is located a distance $\rho_0$ from the center of mass of BC and a distance b (the impact parameter) from the x-axis. $\rho_0$ is a constant chosen such that the atom-diatom interaction potential is essentially zero at this separation. In the present work $\rho_0$ = 4.5 Å, which results in asymptotic ClO+O and $Cl+O_2$ interaction potentials of less than 0.01 kcal/mole. The square of the impact parameter is selected randomly from a uniform distribution with a cutoff at $b \leq b_m$, where $b_m$ is chosen such that the probability of reaction is less than 0.01 for trajectories with $b > b_m$. The standard error associated with this statistical sampling method is minimized if $b_m$ is set at its minimum possible value ($b_m$ = 2.5 Å in the present work). $Q_4^\circ$ is incremented by $\delta Q_4^\circ$, the product of a random fraction of the vibrational period $\tau(v)$ and the relative collision velocity. This ensures that the vibrational phase will be randomly chosen even though all trajectories are started at the vibrational turning points. The $P_i^\circ$ are chosen so that the rotational angular momentum vector of BC has random orientation and magnitude equal to $J(J+1)\hbar^2/R_{BC}^2$, corresponding to the Jth quantum level. The relative momentum between A and BC has magnitude $\{2\mu_{A\text{-}BC}E_{COLL}\}^{1/2}$, where $E_{COLL}$ is the collision energy and is directed along the x-axis ($P_5^\circ = P_6^\circ = 0$).

Thus, the initial conditions are specified for fixed v, J, $E_{COLL}$. The numerical integration is terminated when one of the interatomic distances is greater than $\rho_0 + R^{\circ}_{BC}$.

The total reaction cross section, $S_r$, for fixed v, J, and $E_{COLL}$ is defined by

$$S_r(E_{COLL}, v, J) = \pi b_m^2 \frac{N_r(E_{COLL}, v, J)}{N(E_{COLL}, v, J)} , \qquad \text{(IV-3)}$$

where N is the total number of trajectories and $N_r$ is the number of reactive trajectories. The standard error (one standard deviation) in this statistical sampling scheme is

$$\varepsilon = S_r(E_{COLL}, v, J)\left[\frac{N - N_r}{NN_r}\right]^{1/2} . \qquad \text{(IV-4)}$$

Typically, $N_r < 0.1N$, so that at least 250 trajectories are needed to reduce the sampling error to less than 20%. Thermal rate coefficients K(T) are computed from the thermally weighted reaction cross sections:

$$K(T) = \frac{1}{Q_{v,J}(\pi\mu_{A-BC})^{1/2}}\left(\frac{2}{kT}\right)^{3/2} \sum_{v,J} (2J + 1)\exp(-E_{v,J}/kT)$$

$$\times \int_0^{\infty} S_r(E_{COLL}, v, J)\exp(-E_{COLL}/kT)E_{COLL}\, dE_{COLL} , \qquad \text{(IV-5)}$$

where $Q_{v,J}$ is the exact vibration-rotation partition function, $E_{v,J}$ is the internal energy of BC (v,J) and k is Boltzmann's constant. The electronic degeneracy factor[51] has not been included in Eq. (IV-5) and is discussed in Section V. The summation over v and J can generally be truncated when $E_{v,J} \geq 4kT$ without introducing significant error.

For most non-hydride diatomic molecules the rotational spacings are small and QCT cross sections must be computed for many rotational levels, e.g.,

for ClO rotational levels up to $J = 40$ have appreciable population at 300°K. In an alternate approach, a single set of trajectories can be determined for each value of $v$ and $E_{COLL}$, but with $J$ randomly chosen from a thermal distribution for a given rotational temperature $T_R$.[64] Using this procedure, the computed reaction cross sections are rotationally averaged and can be defined as

$$\bar{S}_r(E_{COLL}, v, T_R) = Q_J^{-1} \sum_J (2J + 1)\exp(-E_J/kT_R)S_r(E_{COLL}, v, J) \quad . \quad (IV-6)$$

Similarly, the rate constant is now given by

$$K(T) = \frac{1}{Q_v(\pi\mu_{A-BC})^{1/2}} \left(\frac{2}{kT}\right)^{3/2} \sum_v \exp(-E_v/kT)$$

$$\times \int_0^\infty \bar{S}_r(E_{COLL}, v, T_R)\exp(-E_{COLL}/kT)E_{COLL}\, dE_{COLL} \quad . \quad (IV-7)$$

This sampling method assumes that vibration and rotation are separable, i.e., $E_{v,J} = E_v + E_J$ and $Q_{v,J} = Q_vQ_J$, which should be valid at low temperatures.

In the present work, rotationally averaged cross sections have been computed using 500 trajectories for each set of initial conditions ($E_{COLL}$, $v$, $T_R$). For a given value of $v$ and $T_R$, these data are then fit to a third-order polynomial in $E_{COLL}$ and the integrals in Eq. (IV-7) are numerically evaluated using Simpson's rule. The error bounds for the rate constants are determined by using $\bar{S}_r(E_{COLL}, v, T_R) \pm \epsilon$ and reevaluating $K(T)$.

The main advantage in using the QCT sampling method is the control one has in selecting the initial conditions. The computed cross sections can be weighted by suitable distribution functions to simulate a wide range of experimental conditions, e.g., thermal system, molecular beam experiment, etc. However, a major disadvantage of the QCT approach is that only a small fraction

of the computed trajectories (usually less than 0.1) are reactive and, as a result, a typical rate constant calculation requires ~10,000 trajectories. A much more efficient procedure for thermal systems, which is also used in the present study, is discussed below.

B. Phase Space Trajectory Sampling Method

The phase space trajectory (PST) sampling method[65-68] is based on Keck's phase space theory.[69] This approach can be much more efficient than the QCT sampling method because the calculation of many nonreactive trajectories is eliminated. In the PST method, trajectories are started in the interaction region of configuration space, where all atoms are in close proximity, and integrated both backward in time to separated reactants, and forward in time to the final species which result from the collision. Most nonreactive trajectories are never examined because they do not reach this interaction region. The details of the method are given in Refs. 65 and 69.

The $6\mathcal{N}$ dimensional phase space, $\Omega$, of a chemical reaction system contains distinct regions that can be identified as reactants $\Omega_R$ and products $\Omega_P$. If a $(6\mathcal{N} - 1)$-dimensional surface S is constructed to completely separate the reactants and products regions of phase space, then the flux of trajectories leaving the reactants region constitutes an upper bound to the rate constant $K_e$. The actual rate constant is obtained by eliminating the contribution to the flux from any nonreactive trajectories which return to the reactants region.

The upper bound rate constant is calculated with the assumption that the system is in the thermochemical equilibrium, i.e., thermal equilibrium exists throughout the entire phase space, according to

$$K_e(T) = Q_R^{-1} \int_{\substack{S=0 \\ V_n>0}} \exp(-E_{TOTAL}/kT) V_n \gamma \prod_{j=1}^{3\mathcal{N}-3} dp_j \prod_{j=2}^{3\mathcal{N}-3} dq_j \ , \qquad \text{(IV-8)}$$

where $V_n$ is the velocity component normal to S and $\gamma = |\nabla S|/(dS/dq_1)$ relates the differential surface area dS to the position coordinates and momenta. $Q_R$ is the reactants classical partition function per unit volume, $\mathcal{V}$, and is defined as

$$Q_R = \mathcal{V}^{-1} \int_{\Omega_R} \exp(-E_{TOTAL}/kT) \prod_{j=1}^{3\mathcal{N}-3} dp_j \, dq_j \ . \qquad \text{(IV-9)}$$

For the 3 body case A + BC it is convenient to use spherical polar coordinates $R_{BC}$, $\phi_{BC}$, $\theta_{BC}$, $R_{A-BC}$, $\phi_{A-BC}$, and $\theta_{A-BC}$ and to choose the dividing surface as $S = q_1 - q_1^*$, where $q_1$ is $R_{BC}$ or $R_{A-BC}$ (in the present study $q_1 = R_{OO}$). Eq. (IV-8) can be simplified to

$$K_e(T) = \left[\frac{2\pi kT}{\mu_{OO}}\right]^{1/2} q_1^{*2} \times \frac{\displaystyle\int_0^{\pi} d\theta_{C1\text{-}OO} \int_{R_{OO}=q_1^*}^{\infty} dR_{C1\text{-}OO} \sin\theta_{C1\text{-}OO} R_{C1\text{-}OO}^2 \exp(-V/kT)}{\displaystyle\int_0^{\infty} dR_{C1O} R_{C1O}^2 \exp[-V_M(R_{C1O})/kT]} \qquad \text{(IV-10)}$$

and the integrals in Eq. (IV-12) can be evaluated numerically using a trapezoidal rule algorithm. The dividing surface is positioned to intersect the reactants' channel of the potential energy surface at $R_{OO}$ = 2.65 Å, the value of $q_1^*$ for which $K_e$ is a minimum at T = 300 °K.

$K_e$ is an upper bound to the rate constant because it includes (1) contributions from those nonreactive trajectories which cross the dividing surface, (2) extra contributions from reactive trajectories which make multiple

crossings of S and (3) contributions from trajectories which originate in the products' region of phase space. To correct $K_e$, classical trajectories are computed with initial conditions corresponding randomly selected points on the dividing surface[70] and integrated forward in time towards products and backward toward reactants according to the scheme given in Ref. 65. The conversion coefficient $\Xi(T)$ is the fraction of "successful" trajectories (i.e., the fraction of reactive trajectories with the elimination of any extra contributions from those trajectories that make multiple crossings of S). Based on this definition, $\Xi$ is a multiplicative correction to $K_e$[67] and the thermal rate constant, K, is given by

$$K(T) = \Xi(T)K_e(T) \qquad \text{(IV-11)}$$

The determination of the conversion coefficient compensates for the assumption of complete equilibrium invoked in Eq. (IV-8)[67] by removing all contributions to the flux which are only present at chemical equilibrium (contribution (3) above). There are no trajectories present in the nonequilibrium case which are absent at chemical equilibrium. The set of "successful" trajectories is equivalent to the set of reactive trajectories which would be obtained in a conventional trajectory calculation, if the initial conditions are sampled from classical thermal distributions (e.g., no zero-point vibrational energy or other features of the QCT sampling method).

The value of K(T), as determined by Eq. (IV-11), does not depend on the choice of S. Thus, minimization of $K_e(T)$ results in maximization of $\Xi$, and minimization of the computational effort required for the calculation of $N_r$ "successful" trajectories. In other words, most of the nonreactive trajectories do not cross the optimal dividing surface especially if S intersects the crest of a barrier on the reaction coordinate. For many systems $\Xi > 0.5$

and values as large as 0.9 have been computed.[65,66] As a result, rate constants and thermal reactant and product distributions can be calculated from only 500 to 1000 total trajectories. The PST method has undergone extensive critical examination and been shown to be equivalent to the conventional classical trajectory method.[67,68] However, for certain systems with large reactant vibrational and rotational spacings the QCT method should be used to correctly account for the effect of quantized initial conditions. The ClO + O system is ideally suited for the PST method because the ClO vibrational spacing is fairly small, and the rotational energy distribution is nearly continuous under low-temperature thermal conditions.

## V. RESULTS

In this section the results of the trajectory calculations using both the QCT and PST sampling methods for reaction (R2a) are presented. The QCT data are for a single ClO rotational temperature of 300 °K. Thermal reaction rate constants, reaction cross sections and activation energies are reported. The results of the PST calculations provide rate constants for the temperature range of 220 to 1000 °K and complement the QCT data. Reagent and product energy distributions have also been determined for reaction (R2a) and these results will be reported separately.

### A. Quasiclassical Trajectory Calculations

In the present work, more than 36,000 quasiclassical trajectories have been computed for reaction (R2a). These calculations used the potential energy surfaces described in section III with $E_{BARR}$ = 0, 0.5, and 1.0 kcal/mole. The initial conditions were specified for values of $E_{COLL}$ between 0.03 and 6.0 kcal/mole, v = 0,1 and J chosen from the thermal ClO rotational

distribution for 300 °K. The rotationally averaged reaction cross sections, rate constants, and average reactant and product energies and scattering angle are summarized in Table V. The variation of bond lengths and bond angle with time for two typical trajectories is shown in Fig. 6.

The rotationally averaged cross sections, $\bar{S}_r(E_{COLL}, v, T_R = 300\ °K)$, were determined for $v = 0$ at numerous collision energies between the apparent threshold[71] and 6 kcal/mole and for $v = 1$ at $E_{COLL} = 1$, 2, 3, and 4 kcal/mole. These data are shown in Fig. 7. The translational energy thresholds for $v = 0$ are zero for $E_{BARR} = 0$ and 0.5 kcal/mole and less than 0.1 kcal/mole for the 1.0 kcal/mole barrier case. Examination of the trajectory data indicates that reactant rotation provides <u>all</u> the additional energy necessary for reaction at low collision energies (i.e., $E_R \geq E_{BARR} - E_{COLL}$ for all reactive trajectories), even though the vibrational zero-point energy (1.223 kcal/mole) could promote the reaction.

Undoubtedly the classical description of the threshold region is not completely accurate owing to the neglect of quantum mechanical phenomena such as tunnelling.[60] However, the most important contributions to the rate constants come from cross sections with $0.4 \leq E_{COLL} \leq 1.5$ kcal/mole, well above the observed threshold values. This is seen by examining plots of the integrand of Eq. (IV-7) which are equivalent to the thermal translational energy distributions for reactive collisions (Fig. 8). The maxima occur at $E_{COLL} \sim 1$ kcal/mole and the magnitudes of the integrands nearer the thresholds are considerably smaller. Since the cross sections for this energy range are large (0.4 to 1.5 Å$^2$), the neglect of quantum threshold effects should not introduce significant errors into the calculated rate constants at temperatures between 200 and 1000 °K. The cross sections computed for ClO(v = 1)

are somewhat higher than the corresponding cross sections for $v = 0$. However, less than 2% of the ClO molecules are in excited vibrational levels at 300 °K and reactive collisions involving vibrationally excited ClO can make only small contributions to the low-temperature thermal rate constants.

The calculated rate constants range from 1.26 to 0.47 × $10^{-11}$ $cm^3$ $mole^{-1}s^{-1}$ as $E_{BARR}$ is varied between zero and 1 kcal/mole. The statistical sampling method introduces an error of about ±15%. These values are a factor of 3 to 5 lower than the recent experimental rate constants for reaction (R2).[17-19] The temperature dependence of the rate constant has been extracted from the 300 °K cross section data by an Arrhenius fit of rate constants calculated at 280 and 320 °K. These values for $E_A$ are only approximate since they are based on the assumption that the cross sections are independent of rotational temperature. The activation energies estimated from the QCT data are greater than 0.5 kcal/mole for all values of $E_{BARR}$, and are in fair agreement with the experimental value of 0.38 kcal/mole determined by Clyne and Nip.[18]

The overall thermal reaction probability, $P_T$, is given by

$$P_T = \frac{\int_o^\infty \exp(-E_{COLL}/kT) E_{COLL} \left[\frac{N_r(E_{COLL},v,T)}{N(E_{COLL},v,T)}\right] dE_{COLL}}{\int_o^\infty \exp(-E_{COLL}/kT) E_{COLL}\, dE_{COLL}} . \qquad (V\text{-}1)$$

where $N_r$ and $N$ are determined as in Eq. (IV-5). At 300 °K 9.2% of the ClO + O collisions are reactive for the zero barrier case. This is in good agreement with the experimental estimate of 10%.[17]

## B. Phase Space Trajectory Calculations

Thermal rate constants and energy distributions have been determined for reaction (R2a) using the phase space trajectory sampling method. In all, over

14,000 phase space trajectories have been computed for $T = 220$, 300, 500, and 1000 °K. These calculations employed potential energy surfaces with $E_{BARR} = 0$, 0.5, and 1 kcal/mole and various forms of $V_\alpha$, the angular dependence. For each of 21 sets of initial conditions (combinations of $T$ and the nature of the potential energy surface) between 50 and 88% of the trajectories are "successful" as compared with less than 10% for typical QCT data. This results in statistical sampling errors of ±2-5% which are considerably smaller than in the QCT calculations because of the greater fraction of reactive trajectories.

The calculated PST rate constants for temperatures between 220 and 1000 °K are shown in Table VI and Fig. 9. The Arrhenius activation energy increases with increasing $E_{BARR}$ and temperature according to

$$E_A \cong E_{BARR} + \frac{k(T_1 + T_2)}{2} \qquad \text{(V-2)}$$

The second term in Eq. (V-2) arises both from the hard sphere temperature dependence $(kT/2)$[22] and from the variation of the potential energy with $\alpha$ in the transition region.

Comparison of the QCT and PST rate constants at 300 °K shows good agreement, especially for the larger values of $E_{BARR}$. Exact agreement between the two methods is not expected because of the differences in selecting the initial conditions. The QCT rate constants are calculated for reactants with thermal quantized rotation and collision energy distributions and fixed vibrational energy (1.223 kcal/mole, corresponding to $v = 0$) while the PST rate constants are determined for fully classical thermal distributions of $E_T$, $E_V$, and $E_R$. The average translation and rotation energies are in close agreement ($\langle E_T \rangle_{QCT} = 1.40$, and $\langle E_T \rangle_{PST} = 1.55$; $\langle E_R \rangle_{QCT} = 0.69$ and $\langle E_R \rangle_{PST} = 0.80$ kcal/mole,

subtle. For example, the ClO vibration frequency might be more rapidly attenuated as the oxygen atom approaches. This would also result in a greater probability of reaction at all temperatures. In the absence of more detailed knowledge of the ClO + O potential energy surface it is difficult to determine the magnitude of $K_2$ to better than a factor of two by theoretical methods since the rate constant is very sensitive to small modifications in the potential energy function. However, these potential surface features affect the preexponential factor much more than the activation energy.

The resulting temperature dependence for reaction (R2) implies that the rate constant for this process is about 20% lower at average stratospheric temperatures than at 300 °K. According to the recent NAS report on stratospheric halocarbons,[13] this would mean a 5% decrease in the predicted amount of odd-oxygen depletion than if a temperature independent value were used for $K_2$. The amounts of stratospheric ClO consumed by reactions (R2) and (R3) would also be slightly shifted. It seems safe to conclude that the body of data for the ClO + O reaction is sufficiently accurate to permit a reliable determination of the rate of stratospheric ozone depletion if all the other necessary kinetic data were available.

## VII. CONCLUSIONS

Rate constants have been computed for reaction

$$ClO + O \rightarrow Cl + O_2 \qquad (R2)$$

for the temperature range 220-1000 °K. The resulting rate constants, $K_2 = 4.36 \times 10^{-11} \exp(-191/T)$ cm$^3$ molecule$^{-1}$ s$^{-1}$, are in good agreement with experimental rate data for 300 °K. The calculated temperature dependence for these rate constants are in excellent agreement with the observations of Clyne and Nip[18] and provide an independent verification of their measurements. The

reaction rate constant at stratospheric temperatures is approximately 20% lower than the room temperature value due to the activation energy of 0.38 kcal/mole. The results demonstrate that classical trajectory calculations based on empirical potential energy surfaces can be used to determine accurate rate constants and activation energies of important atmospheric reactions.

ACKNOWLEDGEMENT

The author is grateful to Dr. L. A. Capone for many helpful discussions on the physics and chemistry of the stratosphere and to Drs. J. O. Arnold and E. E. Whiting for critical discussions on this work and manuscript.

## APPENDIX: PARAMETERIZATION OF THE BENDING POTENTIAL

The double minimum function given in Eq. (III-4),

$$Y = A(\alpha - \pi)^2 + \frac{B}{C + (\alpha - \pi)^2} + D \ , \qquad \text{(A-1)}$$

is parameterized as follows. Fixing the minima at the equilibrium bond angles $\alpha_e$ and $(2\pi - \alpha_e)$ implies

$$(\alpha_e - \pi)^2 = -C + \sqrt{B/A} \ , \qquad \text{(A-2)}$$

and

$$A(\alpha_e - \pi)^2 + \frac{B}{C + (\alpha_e - \pi)^2} + D = 0 \ , \qquad \text{(A-3)}$$

since $Y(\alpha_e) = 0$. The maximum occurs when $\alpha = \pi$ and $Y = E^*$ which yields a third equation:

$$E^* = B/C + D \qquad \text{(A-4)}$$

Finally the second derivative of $Y$ at the minimum, equals the bending force constant $f_B$:

$$f_B = 2A + \frac{2B\{3(\alpha_e - \pi)^2 - C\}}{\{C + (\alpha_e - \pi)^2\}^3} \ . \qquad \text{(A-5)}$$

Equations (A-2)-(A-5) comprise a set of four simultaneous algebraic equations in four unknowns (A, B, C, and D). The solution of these equations is given below:

$$A = f_B E^*/\Gamma \ , \tag{A-6}$$

$$B = \frac{64 f_B E^{*3} (\alpha_e - \pi)^4}{\Gamma^3} \tag{A-7}$$

$$C = \frac{f_B (\alpha_e - \pi)^4}{\Gamma} \tag{A-8}$$

and

$$D = \frac{f_B E^* (\alpha_e - \pi)^2 [f_B (\alpha_e - \pi)^2 - 16E^*]}{\Gamma^2} \ ; \tag{A-9}$$

where $\Gamma$ is defined by

$$\Gamma = 8E^* - f_B (\alpha_e - \pi)^2 \ . \tag{A-10}$$

REFERENCES


*NASA/NRC Research Associate 1974-1976.

[1]M. J. Molina and F. S. Rowland, Nature 249, 810 (1974).

[2]F. S. Rowland and M. J. Molina, Rev. Geophys. Space Phys. 13, 1 (1975).

[3]$CFCl_3$ has been detected in the stratosphere at altitudes between 10 and 40 km. See: J. E. Lovelock, Nature 252, 292 (1974); N. E. Hester, E. R. Stephens and O. C. Taylor, Atmos. Envir. 9, 603 (1975); L. E. Heidt, R. Lueb, W. Pollock and D. H. Ehhalt, Geophys. Res. Lett. 2, 445 (1975).

[4]R. J. Cicerone, R. S. Stolarski, and S. Walters, Science 185, 1165 (1974).

[5]S. C. Wofsy, M. B. McElroy, and N. D. Sze, Science 187, 535 (1975).

[6]R. P. Turco and R. C. Whitten, Atmos. Envir. 9, 1045 (1975).

[7]P. Crutzen, Geophys. Res. Lett. 1, 205 (1974).

[8]R. T. Watson, Chemical Kinetics Data Survey, VIII, Rate Constants of $ClO_x$ of Atmospheric Interest, NBSIR 74-516, National Bureau of Standards, Washington, D.C., 1974; J. Chem. and Phys. Ref. Data 6, 871 (1977).

[9]R. D. Hudson, editor, Chlorofluoromethanes and the Stratosphere (NASA, Washington, D.C., 1977).

[10]R. S. Stolarski and R. J. Cicerone, Can. J. Chem. 52, 1610 (1974).

[11]S. C. Wofsy and M. B. McElroy, Can. J. Chem. 52, 1582 (1974).

[12]P. Crutzen, Can. J. Chem. 52, 1569 (1974).

[13]Halocarbons: Effects on Stratospheric Ozone (National Academy of Sciences-National Research Council, Washington, D.C., 1977).

[14]M. A. A. Clyne and J. A. Coxon, Trans. Far. Soc. 62, 1175 (1966).

[15]N. Basco and S. K. Dogra, Proc. Roy. Soc. A. 323, 29, 401 (1971).

[16]G. C. Freeman and L. F. Phillips, J. Phys. Chem. 72, 3025 (1968).

[17]P. P. Bemand, M. A. A. Clyne, and R. T. Watson, J. Chem. Soc. Farad. I 69, 1356 (1973).

[18]M. A. A. Clyne and W. S. Nip, J. Chem. Soc. Faraday Trans. I 72, 2211 (1976).

[19]M. S. Zahniser and F. Kaufman, J. Chem. Phys. 66, 3673 (1977).

[20]C. Park, J. Phys. Chem. 80, 565 (1976).

[21]The temperature dependence of the rate constant is defined as $-kd\ \ell n\ K/d\ 1/T$. The activation energy $E_A$ equals this temperature dependence when defined as $K = A \exp(-E_A/kT)$. If $K$ is written as $AT^q \exp(-E_A/kT)$ then the temperature dependence is equal to $E_A + qkT$.

[22]The collision theory expression for a bimolecular rate constant equals $S_r[8\pi kT/\mu]^{1/2}$ where $S_r$ is the hard-sphere cross section and $\mu$ is the reduced mass. For the general case this $T^{1/2}$ dependence will remain unless $S_r$ is an explicit function of temperature. As a result, there will always

be a contribution of (1/2)kT to the apparent activation energy of a gas phase bimolecular reaction which arises from the temperature dependence of the collision frequency.

[23]M. A. A. Clyne and R. T. Watson, J. Chem. Soc. Farad I 70, 2250 (1974).

[24]M. A. A. Clyne, D. J. McKenney, and R. T. Watson, J. Chem. Soc. Farad. I 71, 322 (1975).

[25]H. S. Johnston, E. D. Morris, and J. van den Bogaerde, J. Am. Chem. Soc. 91, 7712 (1969).

[26]R. A. Durie and D. A. Ramsay, Can. J. Phys. 36, 35 (1958).

[27](a) J. A. Coxon, W. E. Jones, and E. G. Skolnik, Can. J. Phys. 54, 1043 (1976);
(b) J. A. Coxon and D. A. Ramsay, Can. J. Phys. 54, 1034 (1976).

[28](a) D. M. Cooper, J. Quant. Spectr. and Rad. Transfer 17, 543 (1977);
(b) S. R. Langhoff, R. L. Jaffe, and J. O. Arnold, J. Quant. Spectr. and Rad. Transfer 18, 227 (1977).

[29]M. Karplus, R. N. Porter, and R. D. Sharma, J. Chem. Phys. 43, 3259 (1965).

[30]R. L. Jaffe and J. B. Anderson, J. Chem. Phys. 54, 2224 (1971); ibid. 56, 682 (1972).

[31]J. T. Muckerman, J. Chem. Phys. 54, 1155 (1971); ibid. 56, 2997 (1972); ibid. 57, 3388 (1972).

[32]R. L. Wilkins, J. Chem. Phys. 57, 912 (1972).

[33]JANAF Thermochemical Tables, NSRDS-NBS 37 (National Bureau of Standards, Washington, 2nd ed., 1971).

[34]B. Rosen, Spectroscopic Data Relative to Diatomic Molecules (Pergamon, Oxford, 1970).

[35]N. Basco and R. D. Morse, J. Mol. Spect. 45, 35 (1973).

[36]J. O. Arnold, E. E. Whiting, and S. R. Langhoff, J. Chem. Phys. 66, 4459 (1977).

[37]G. Herzberg, Spectra of Diatomic Molecules (Van Nostrand, New York, 2nd ed., 1950), Chap. 3.

[38]C. E. Moore, Atomic Energy Levels, Circular 467 (National Bureau of Standards, Washington, 1958).

[39]F. J. Lipscomb, R. G. W. Norrish, and B. A. Thrush, Proc. Roy. Soc. A. 233, 455 (1956).

[40]N. Basco and S. K. Dogra, Proc. Roy. Soc. A. 323, 29 (1971).

[41]N. Basco and R. D. Morse, Proc. Roy. Soc. A. 336, 495 (1971).

[42]P. J. Kuntz, E. M. Nemeth, J. C. Polanyi, S. D. Rosner, and C. E. Young, J. Chem. Phys. 44, 1168 (1966).

[43]J. C. Polanyi, Acc. Chem. Res. 5, 161 (1972).

[44]S. W. Benson and J. H. Buss, J. Chem. Phys. 27, 1382 (1957).

[45]A. Arkell and I. Schwager, J. Am. Chem. Soc. 89, 5999 (1967).

[46]R. W. Eachus, P. R. Edwards, S. Subramanian, and M. C. R. Symons, J. Chem. Soc., 1704 (1968).

[47]J. L. Gole and E. F. Hayes, Int. J. Quant. Chem. 3S, 519 (1970).

[48]R. L. Jaffe, unpublished data.

[49]D. D. Wagman and D. Garvin, Provisional Thermochemical Data Sheets for ClO and ClOO (National Bureau of Standards, Washington, 1974).

[50]K. E. Shuler, J. Chem. Phys. 21, 624 (1953).

[51]J. T. Muckerman and M. D. Newton, J. Chem. Phys. 56, 3191 (1972).

[52]G. Herzberg, Electronic Spectra and Electronic Structure of Polyatomic Molecules (Van Nostrand, New York, 1966).

[53]Strictly speaking the noncrossing rule applies only to diatomic systems. However, the allowed intersection of states of the same symmetry is still very improbable in polyatomic systems. For a discussion of this point see: T. F. George, K. Morokuma and Y. W. Lin, Chem. Phys. Lett. 30, 54 (1975).

[54]For a review of the theory of nonadiabatic collisions see: E. E. Nikitin, in Physical Chemistry, an Advanced Treatise, W. Jost, editor (Academic Press, New York, 1974), Vol. 6, 187.

[55]S. Sato, J. Chem. Phys. 23, 592, 2465 (1955).

[56]J. C. Polanyi and J. L. Schreiber, Disc. Farad. Soc. 55, 372 (1973).

[57]N. C. Blais and D. G. Truhlar, J. Chem. Phys. 61, 4186 (1974).

[58]The observed chemical stability of OClO means that ClOO and OClO must be separated by a sizeable potential energy barrier. Since processes involving OClO are not of interest in the present work the empirical potential energy surface constructed for the study of reaction (R2a) does not include the well corresponding to a stable OClO species.

[59]J. T. Vanderslice, E. A. Mason, and W. G. Maisch, J. Chem. Phys. 32, 515 (1960).

[60]For comparisons between quantum and classical calculations of chemical reaction dynamics see: J. M. Bowman and A. Kuppermann, Chem. Phys. Lett. 19, 166 (1973); G. C. Schatz, J. M. Bowman, and A. Kuppermann, J. Chem. Phys. 63, 674, 685 (1975).

[61]J. T. Muckermann, Quantum Chemistry Program Exchange #229, Indiana University, 1973.

[62]P. Brumer and M. Karplus, Disc. Farad. Soc. 55, 80 (1973).

[63]R. N. Porter, Ann. Rev. Phys. Chem. 25, 317 (1974).

[64]L. M. Raff, D. L. Thompson, L. B. Sims, and R. N. Porter, J. Chem. Phys. 56, 5998 (1972).

[65]R. L. Jaffe, J. M. Henry, and J. B. Anderson, J. Chem. Phys. 59, 1128 (1973); J. M. Henry, J. B. Anderson, and R. L. Jaffe, Chem. Phys. Lett. 20, 138 (1973).

[66]R. L. Jaffe, J. M. Henry, and J. B. Anderson, J. Am. Chem. Soc. 98, 1140 (1976).

[67]J. B. Anderson, J. Chem. Phys. 58, 4684 (1973); J. B. Anderson, ibid. 62, 2446 (1975).

[68]R. N. Porter, D. L. Thompson, L. M. Raff, and J. M. White, J. Chem. Phys. 62, 2429 (1975).

[69]J. C. Keck, Adv. Chem. Phys. 13, 85 (1967).

[70]The initial coordinates and momenta are chosen with a weighting that reflects the magnitude of the integrand in Eq. (IV-12) with $R_{OO} = q_1^*$. This means each pair $(R_{Cl-OO}, \theta_{Cl-OO})$ has a statistical weight given by $[\sin \theta_{Cl-OO} R^2_{Cl-OO} \exp(-V/kT)]$, the other coordinates are chosen from uniform distributions and the momenta are selected from Maxwellian distributions.

[71]The apparent threshold energy in a trajectory calculation is usually defined as the minimum collision energy for which $N_r/N > 0$. Since $N$ is generally less than 1000 the reaction probability at the apparent threshold is greater than $10^{-3}$. This apparent threshold approaches the true threshold energy as $N$ becomes very large. In the present work a lower limit of 0.03 kcal/mole has been imposed on the apparent threshold energy.

[72]Under these modifications the potential energy surface is not accurate in the triatomic region ($V_{III}$). This will not affect the rate constants since any phase space trajectories which reach region III will certainly be

reactive. However, the product energy distributions depend on the breakup of the ClOO complex and will be affected by changes to $E^{*\prime}$ and $f_B'$. In fact, reduction of the bending force constant to $f_B/4$ results in a 15 to 20% increase in the amount of energy channeled into product vibration.

[73]D. G. Truhlar, J. Chem. Phys. 56, 3189 (1972).

[74]R. L. Jaffe, Ph.D. Thesis, Yale University, 1973.

[75]A. Komornicki, K. Morokuma, and T. F. George, J. Chem. Phys. 67, 5012 (1977).

TABLE I. Physical constants for ClO and $O_2$

| | $ClO(^2\Pi)$[a] | $O_2(^3\Sigma_g^-)$[b] | $O_2(^1\Delta_g)$[b] | $O_2(^1\Sigma_g^+)$[b] |
|---|---|---|---|---|
| $D_o$, kcal/mole | 63.31[c] (63.427) | 117.97 | 95.43 | 80.45 |
| $r_e$, Å | 1.546[d] (1.56965) | 1.20739[e] | 1.2157 | 1.22685 |
| $\omega_e$, $cm^{-1}$ | 859 (853.8) | 1580.211 | 1509.3 | 1432.6874 |
| $\omega_e x_e$, $cm^{-1}$ | 6.8 (5.5) | 11.99 | 12.9 | 13.95008 |
| $E_{v=0}$, kcal/mole | 1.223 | 2.250 | 2.148 | 2.038 |
| $\Delta E(v = 1 \leftarrow 0)$, kcal/mole | 2.417 | 4.449 | --- | --- |
| $B_e$, $cm^{-1}$ | 0.643[f] (0.62345) | 1.445572 | 1.4264 | 1.4004 |
| $E_{J=20}$, kcal/mole | 0.767[f] | 1.724 | --- | --- |

[a] From Ref. 35, unless specified otherwise. Values in parentheses are from Coxon, Jones and Skolnik[27a] and were not available until the present calculations were completed.

[b] From Ref. 34, unless specified otherwise.

[c] From Ref. 26.

[d] From Ref. 34.

[e] From Ref. 37.

[f] From Ref. 33.

TABLE II. Relative collision frequencies for $ClO(^2\Pi) + O(^3P_g)$ fine structure states

| | T = 220 °K | T = 300 °K | T = 1000 °K |
|---|---|---|---|
| $ClO(^2\Pi_{3/2}) + O(^3P_2)$ | 0.761 | 0.674 | 0.410 |
| $ClO(^2\Pi_{3/2}) + O(^3P_1)$ | 0.162 | 0.189 | 0.196 |
| $ClO(^2\Pi_{3/2}) + O(^3P_0)$ | 0.035 | 0.045 | 0.059 |
| $ClO(^2\Pi_{3/2}) + O(^3P_g)$ | 0.958 | 0.908 | 0.765 |
| $ClO(^2\Pi_{1/2}) + O(^3P_2)$ | 0.033 | 0.068 | 0.207 |
| $ClO(^2\Pi_{1/2}) + O(^3P_1)$ | 0.007 | 0.019 | 0.099 |
| $ClO(^2\Pi_{1/2}) + O(^3P_0)$ | 0.002 | 0.005 | 0.030 |
| $ClO(^2\Pi_{1/2}) + O(^3P_g)$ | 0.042 | 0.092 | 0.336 |

TABLE III. Physical constants for ClOO and OClO

| | ClOO[a] | OClO |
|---|---|---|
| $R_{ClO}$, Å | 1.83 | 1.47[b] |
| $R_{OO}$, Å | 1.23 | --- |
| α | 110° | 118°[b] |
| E(0,0,0), kcal/mole | 3.18 | 3.58[c] |
| $\omega_1$, $cm^{-1}$ | 1440.8[d] | 945.3[c] |
| $\omega_2$, $cm^{-1}$ | 407[d] | 447.4[c] |
| $\omega_3$, $cm^{-1}$ | 373[d] | 1109[c] |

[a]Data from Ref. 45.

[b]Data from: M. C. K. Pillai and R. F. Curl, J. Chem. Phys. 37, 2921 (1962).

[c]Data from Ref. 33.

[d]The corresponding force constants are $f_{OO}$ = 9.65 mdyne/Å, $f_{OCl}$ = 1.29 mdyne/Å, $f_{OOCl}$ = 1.04 mdyne Å, $f_{OCl-OOCl}$ = 0.54 mdyne, $f_{OO-OCl}$ = 0.07 mdyne/Å.

TABLE IV. Potential surface parameters.

| | $D_e$, kcal/mole | $\beta$, $Å^{-1}$ | $R_e$, Å |
|---|---|---|---|
| ClO ($V_I$) | 64.553 | 2.31153 | 1.546 |
| $O_2$ ($V_V$) | 120.217 | 2.62747 | 1.20739 |
| OO in ClOO ($V_{III}$) | 63.592 | 3.3132 | 1.23 |
| ClO in ClOO ($V_{III}$) | 7.765 | 3.4577 | 1.83 |

| | E*, kcal/mole | $f_B$, mdyne Å | $\alpha_e$ |
|---|---|---|---|
| ClOO bend ($V_{III}$) | 70. | 1.04 | 110° |

| | $\rho$, Å | $\lambda$, Å | $V_p$, kcal/mole |
|---|---|---|---|
| $V_{II}$ | 2.6 | 0.4 | 3.0, 2.5, 2.0[a] |
| $V_{IV}$ | 3.4 | 0.3 | 0.5 |

[a]The values of $V_p$ correspond to $E_{BARR}$ = 0, 0.5, and 1.0 kcal/mole, respectively.

TABLE V. Summary of QCT results[a]

| | $E_{BARR} = 0$ | $E_{BARR} = 0.5$ | $E_{BARR} = 1.0$ |
|---|---|---|---|
| N | 8917 | 12486 | 10444 |
| $N_r$ | 811 | 753 | 411 |
| $P_T$ | 0.092 | 0.054 | 0.030 |
| K | $1.27\pm0.18\times10^{-11}$ | $0.78\pm0.13\times10^{-11}$ | $0.47\pm0.11\times10^{-11}$ |
| $E_A$[b] | 0.50 | 0.60 | 0.77 |
| $\langle J \rangle$ | 17 | 18 | N.D.[c] |
| $\langle \theta \rangle$ | 98° | 101° | N.D. |
| $\langle v' \rangle$ | 7.5 | 7.6 | N.D. |
| $\langle E'_T \rangle$ | 19.36(33%)[d] | 22.66(38%) | N.D. |
| $\langle E'_V \rangle$ | 32.43(55%) | 31.23(53%) | N.D. |
| $\langle E'_R \rangle$ | 6.72(12%) | 5.19(9%) | N.D. |

[a]Energies are in kcal/mole, rate constants in $cm^3$ $molecule^{-1}$ $s^{-1}$ and angles in degrees. All other quantities are dimensionless. All data is for 300 °K.

[b]Determined from rate constants calculated using Eq. (IV-7) for T = 280 to 320 °K. This assumes that the averaged cross-sections are independent of rotational temperature.

[c]Quantities marked N.D. were not determined.

[d]Quantities in parentheses are percentages of the total energy.

[e]The experimentally determined value for $\langle E'_V \rangle$ is 25 kcal/mole (45%), as given in Ref. 41.

TABLE VI. PST rate constant data.

| T, °K | $E_{BARR}$ = 0[a] | $E_{BARR}$ = 0.5 kcal/mole[a] | $E_{BARR}$ = 1.0 kcal/mole[b] |
|---|---|---|---|
| I. | $K_e \times 10^{11}$ cm$^3$molecule$^{-1}$s$^{-1}$ | | |
| 220 | 2.007 | 0.685 | 0.234 |
| 300 | 2.828 | 1.286 | 0.585 |
| 500 | 4.893 | 3.050 | 1.901 |
| 1000 | 10.116 | 7.986 | 6.305 |
| II. | $\tilde{\tau}$ | | |
| 220 | 0.747 | 0.824 | 0.874 |
| 300 | 0.757 | 0.815 | 0.850 |
| 500 | 0.759 | 0.795 | 0.810 |
| 1000 | 0.679 | 0.706 | 0.692 |
| III. | $K \times 10^{11}$ cm$^3$molecule$^{-1}$s$^{-1}$ | | |
| 220 | 1.499±0.028 | 0.565±0.008 | 0.205±0.003 |
| 300 | 2.141±0.038 | 1.048±0.027 | 0.497±0.016 |
| 500 | 3.724±0.066 | 2.425±0.039 | 1.540±0.033 |
| 1000 | 6.869±0.149 | 5.638±0.115 | 4.363±0.130 |

[a]Data based on samples of 1000 trajectories.

[b]Data based on samples of 500 trajectories.

TABLE VII. Variation of the angular dependence of the potential energy surface.[a,b]

| T | E*' kcal/mole | $f_B'$ [c] | $K_e \times 10^{11}$ $cm^3 molecule^{-1} s^{-1}$ | $\approx$ | $K \times 10^{11}$ $cm^3 molecule^{-1} s^{-1}$ |
|---|---|---|---|---|---|
| 220 °K | 40 | $f_B$ | 2.008 | 0.736 | 1.478±0.040 |
| | 70 | $f_B$ | 2.007 | 0.747 | 1.499±0.028 |
| | 70 | $f_B/2$ | 2.835 | 0.644 | 1.826±0.061 |
| | 70 | $f_B/4$ | 4.001 | 0.597 | 2.389±0.113 |
| 300 °K | 40 | $f_B$ | 2.830 | 0.680 | 1.924±0.059 (0.43)[d] |
| | 70 | $f_B$ | 2.828 | 0.757 | 2.141±0.038 (0.58)[d] |
| | 70 | $f_B/2$ | 3.993 | 0.578 | 2.308±0.088 (0.38)[d] |
| | 70 | $f_B/4$ | 5.633 | 0.513 | 2.890±0.162 (0.31)[d] |
| 1000 °K | 40 | $f_B$ | 10.139 | 0.686 | 6.956±0.210 |
| | 70 | $f_B$ | 10.116 | 0.679 | 6.869±0.149 |
| | 70 | $f_B/2$ | 14.309 | 0.502 | 7.183±0.320 |
| | 70 | $f_B/4$ | 20.605 | 0.527 | 10.852±0.594 |

[a] Data based on samples of 500 trajectories except $E^{*\prime} = 70$, $f_B' = f_B$ case (1000) and $E^{*\prime} = 70$, $f_B' = f_B/4$ case (300).

[b] $E_{BARR} = 0$.

[c] The values of $f_B'$ are given in terms of $f_B = 1.04$ mdyne Å, the experimental bending force constant for C100.

[d] The values in parentheses are the activation energies in kcal/mole as determined from the 220 and 300° data. The lower limit (hard sphere case) is 0.26 kcal/mole.

## FIGURE CAPTIONS

Fig. 1. Energy diagram for the $ClO_2$ system. The energies are in kcal/mole relative to separated ClO ($^2\Pi_{3/2}$) + O($^3P_g$).

Fig. 2. Adiabatic electronic correlations between low-lying states of ClO + O, ClOO, and Cl + $O_2$. Electronic states of ClOO denoted by dashed lines have not been observed experimentally or theoretically.

Fig. 3. Schematic partitioning of the ground state ClOO potential energy surface for $\alpha = \alpha_e$. Regions I and V correspond to separated atom-diatom configurations and region III corresponds to triatomic configurations. The transition regions are II and IV. $V_A$ is determined from $V_I$ for $R_{OO} > 2.2$ Å and $V_B$ is determined by an interpolation between $V_{III}$ and $V_V$ for $R_{OO} < 3.0$ Å. The potential in region IV is specified by $V_B$ for $3.1 < R_{Cl\text{-}OO} < 3.7$ Å and the potential in region II is specified by an interpolation between $V_A$ and $V_B$. The reaction coordinate for ClO + O → Cl + $O_2$ is also shown. The barrier is located at ◊ and the ClOO equilibrium geometry is located at o.

Fig. 4. Contour plots of the ground state ClOO potential energy surface for $E_{BARR} = 0$. The energy contours are in kcal/mole relative to separated ClO + O. The bond angle $\alpha$ is fixed as follows for each plot: (a) $\alpha = 90°$, (b) $\alpha = \alpha_e = 110°$, and (c) $\alpha = 130°$. The ClOO equilibrium geometry is located at ◊ in (b).

Fig. 5. The parameters used to specify the initial coordinates for the quasi-classical trajectory sampling method. $\delta Q_4^\circ$ is the displacement of atom A along the -x axis to effect randomization of the initial vibrational phase of BC.

Fig. 6. Typical reactive trajectory. (a) Variation of bond lengths and bond angle with time for a trajectory with $E_{COLL} = 1.0$ kcal/mole, $E_{BARR} = 0$. The encounter time is $4.2 \times 10^{-13}$ s. (b) Path of this trajectory in $(R_{ClO}, R_{OO})$ space superimposed on the potential surface with $\alpha = \alpha_e$. Selected points labeled a through e are shown in both (a) and (b).

Fig. 7. Rotationally averaged reactive cross sections for $ClO + O \rightarrow Cl + O_2$ at 300 °K. The points denoted by ◊ and o are for $v = 0$ and $v = 1$, respectively. The smooth curves are polynomial least square fits to the $v = 0$ data. Statistical error limits are shown for the $v = 0$ data. The results are for: (a) $E_{BARR} = 0$, (b) $E_{BARR} = 0.5$, and (c) $E_{BARR} = 1.0$ kcal/mole.

Fig. 8. Translational energy distributions for reactive trajectories. $F(E_{COLL}) \cdot \bar{S}_r(E_{COLL}, v = 0, T = 300\ °K)$. The polynomial least squares fits to the rotationally averaged cross sections were used. The dashed curve is the distribution for all collisions, $F(E_{COLL})$.

Fig. 9. Arrhenius plot of the rate constant data for $ClO + O \rightarrow Cl + O_2$. The solid curves are calculated PST rate constants. The dashed curve is the "best" PST result for $E_{BARR} = 0$ and $f_B' = f_B/2$. The points represent experimental measurements: (a) Bemand, Clyne and Watson,[17] (b) Clyne and Nip[18] (....), (c) Zahniser and Kaufman[19] (-·-), (d) Freeman and Phillips,[16] (e) Basco and Dogra,[15] and (f) Park.[20]

Fig. 10. Contours of equal potential energy as a function of $R_{ClO}$ and $\alpha$ with $R_{OO} = q_1^* = 2.65$ Å for $E_{BARR} = 0$. The contours are for $V = 1$, 5 and 10 kcal/mole. The dashed lines are for $R_{ClO} = R_e$ and $\alpha = \alpha_e$. (a) $E^* = 70$ kcal/mole and $f_B' = f_B$. (b) $E^* = 70$ kcal/mole and $f_B' = f_B/4$.

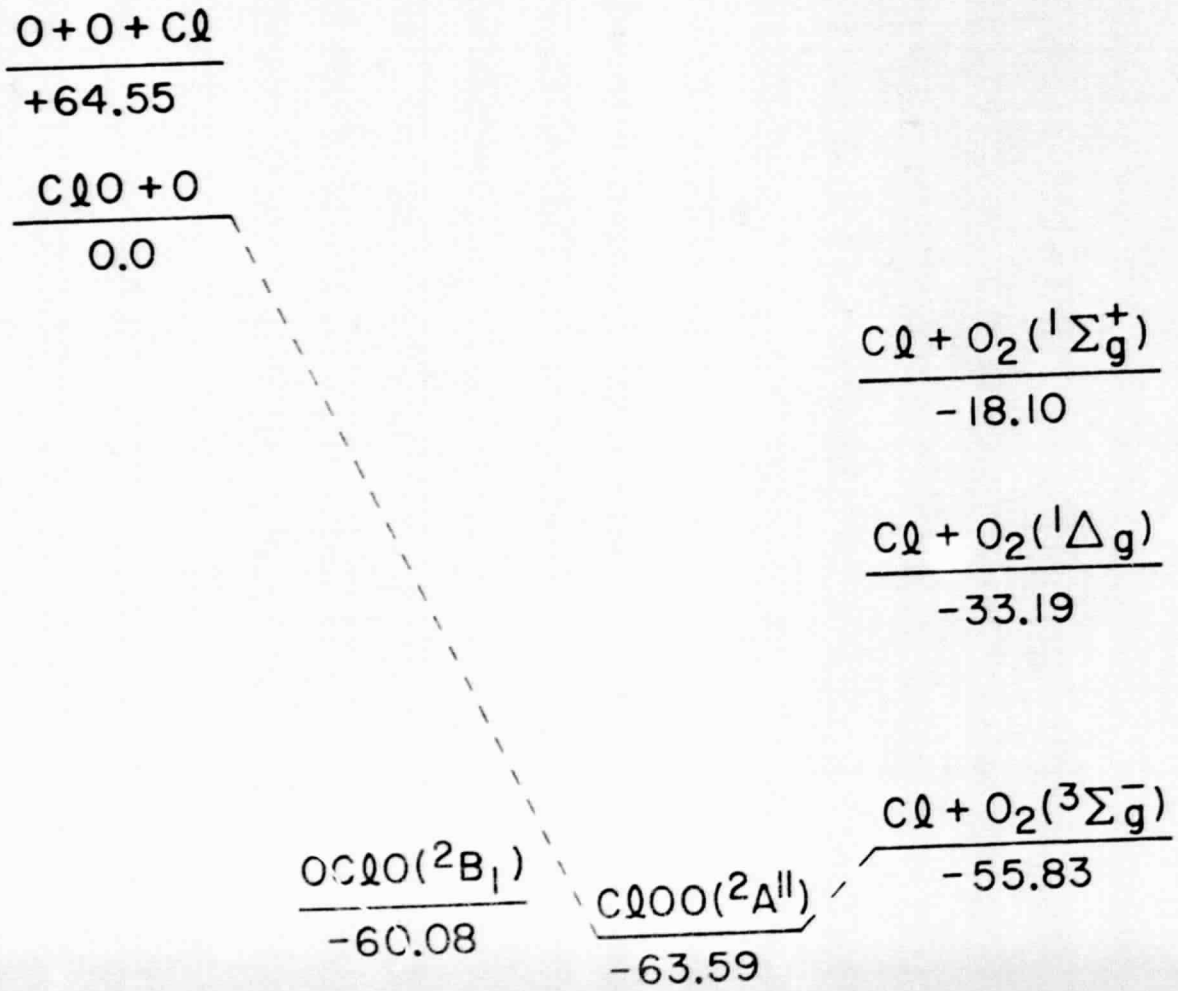
O + O + Cl
+64.55
ClO + O
0.0
Cl + O2(1Σg+)
-18.10
Cl + O2(1Δg)
-33.19
Cl + O2(3Σg−)
-55.83
OClO(2B1)
-60.08
ClOO(2A'')
-63.59

Fig. 1

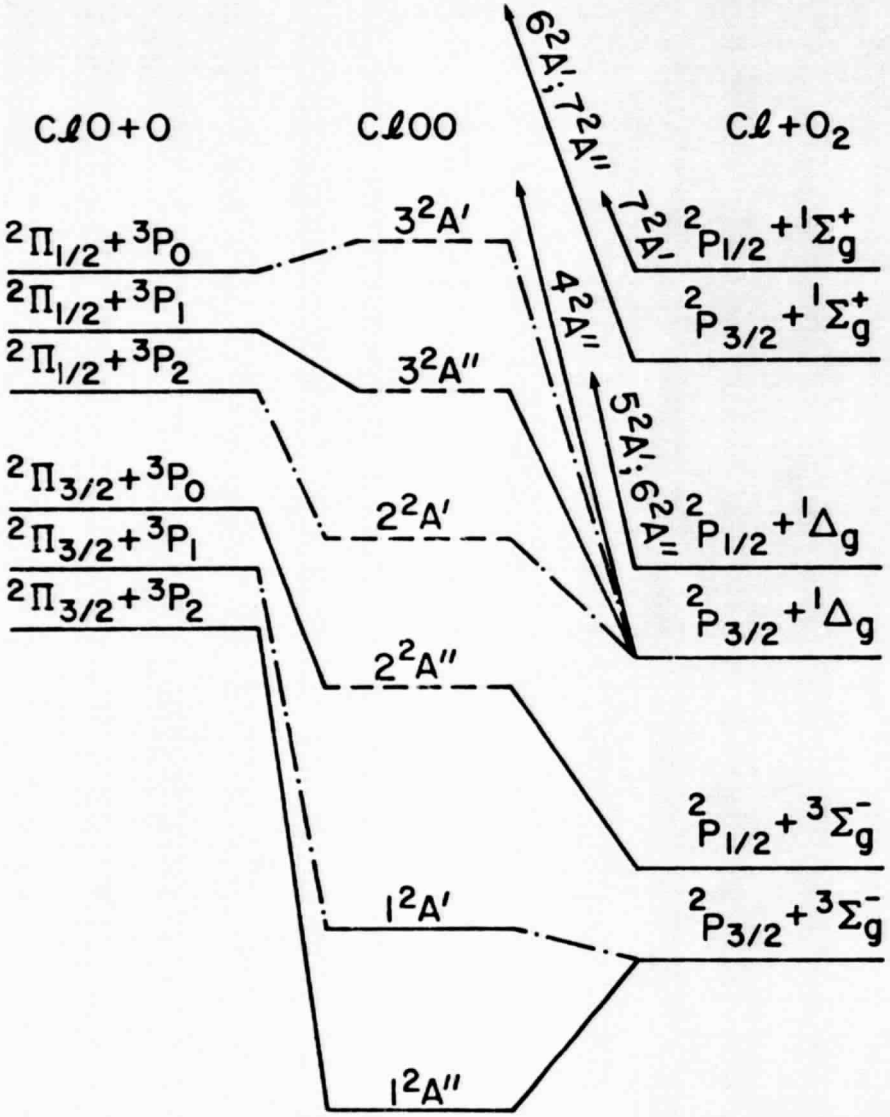
ClO+O
ClOO
Cl+O2
$^2\Pi_{1/2}+^3P_0$
$^2\Pi_{1/2}+^3P_1$
$^2\Pi_{1/2}+^3P_2$
$^2\Pi_{3/2}+^3P_0$
$^2\Pi_{3/2}+^3P_1$
$^2\Pi_{3/2}+^3P_2$
$3^2A'$
$3^2A''$
$2^2A'$
$2^2A''$
$1^2A'$
$1^2A''$
$6^2A';7^2A''$
$7^2A'$
$4^2A''$
$5^2A';6^2A''$
$^2P_{1/2}+^1\Sigma_g^+$
$^2P_{3/2}+^1\Sigma_g^+$
$^2P_{1/2}+^1\Delta_g$
$^2P_{3/2}+^1\Delta_g$
$^2P_{1/2}+^3\Sigma_g^-$
$^2P_{3/2}+^3\Sigma_g^-$

Fig. 2

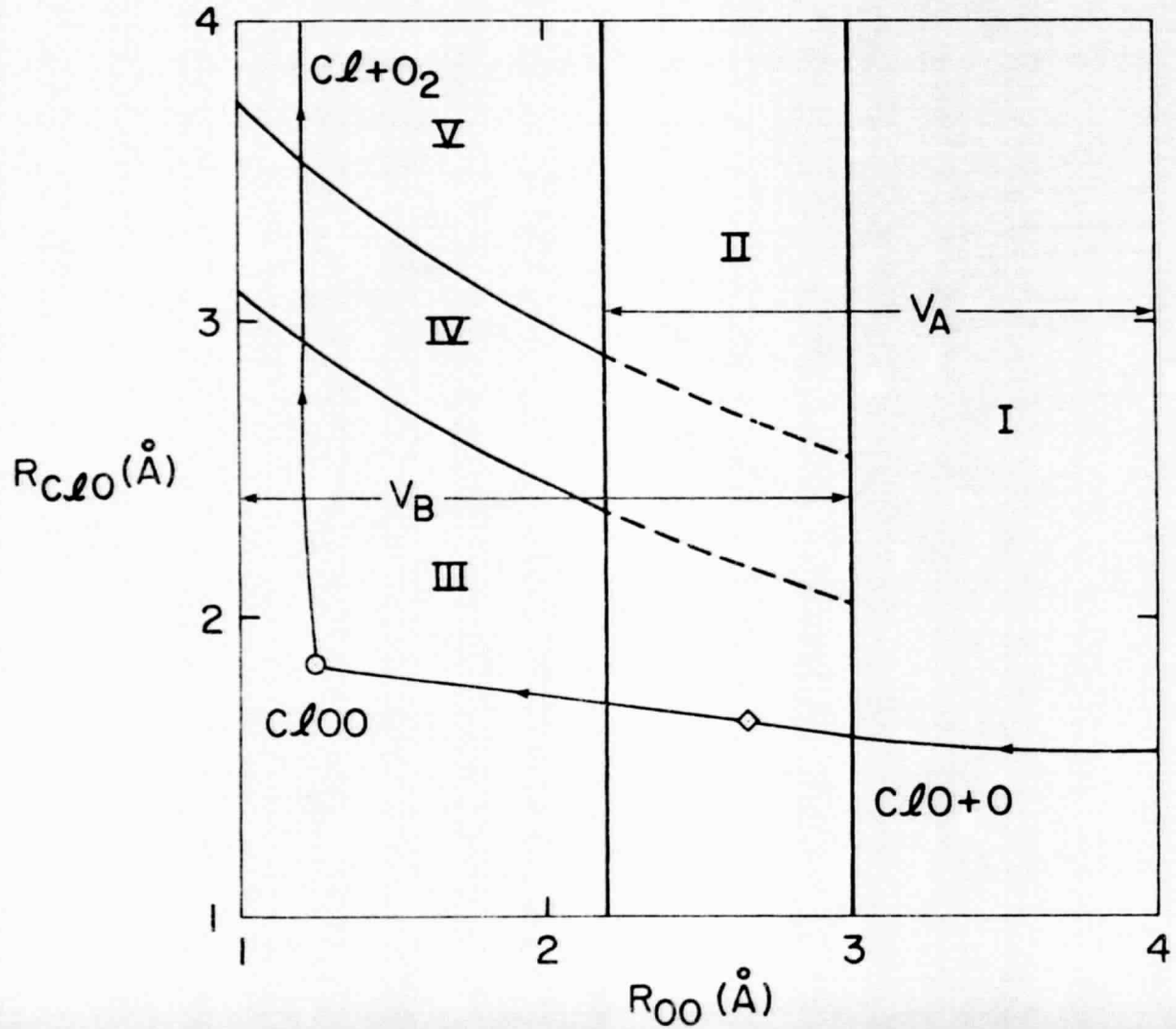


Fig. 3

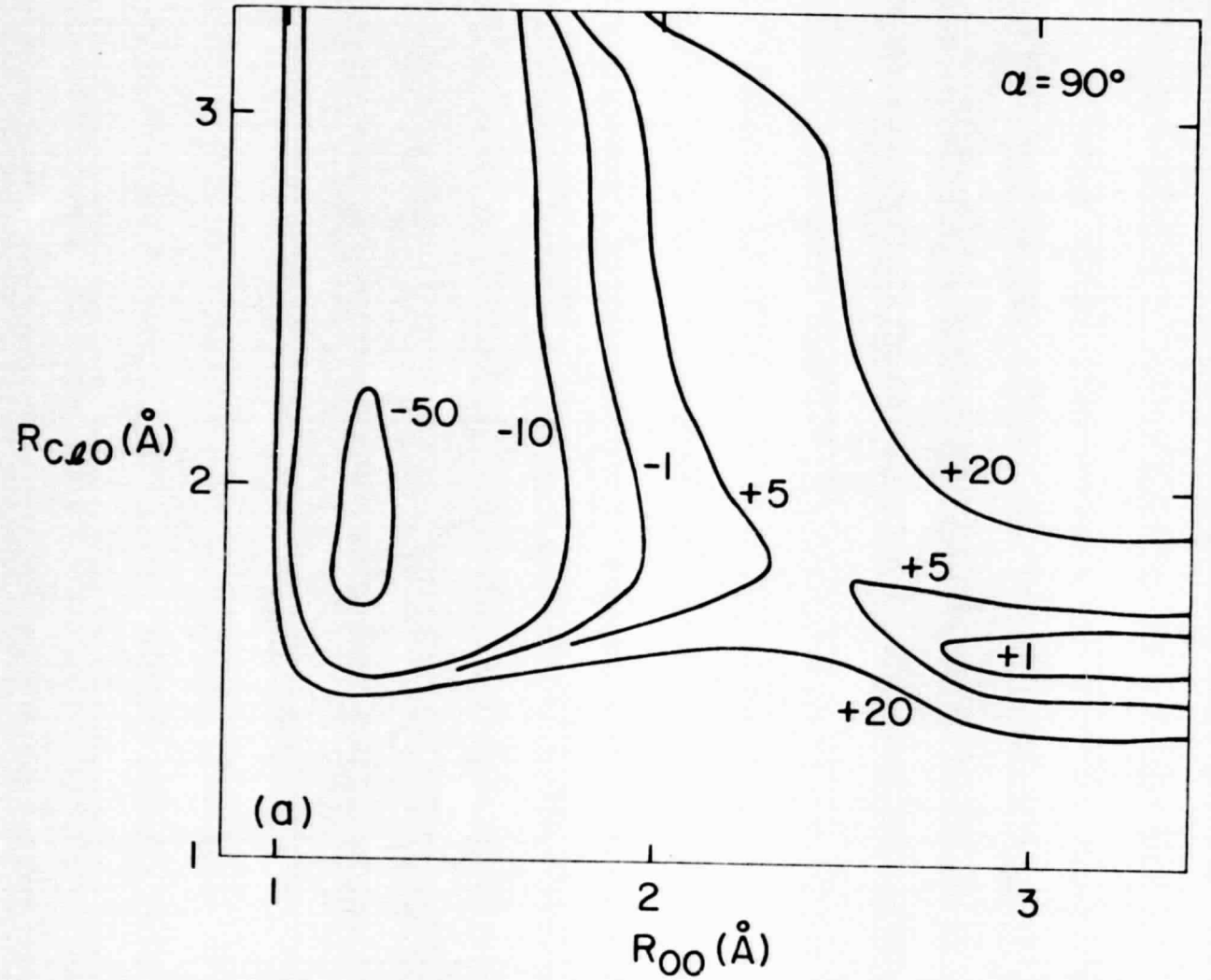


Fig. 4a

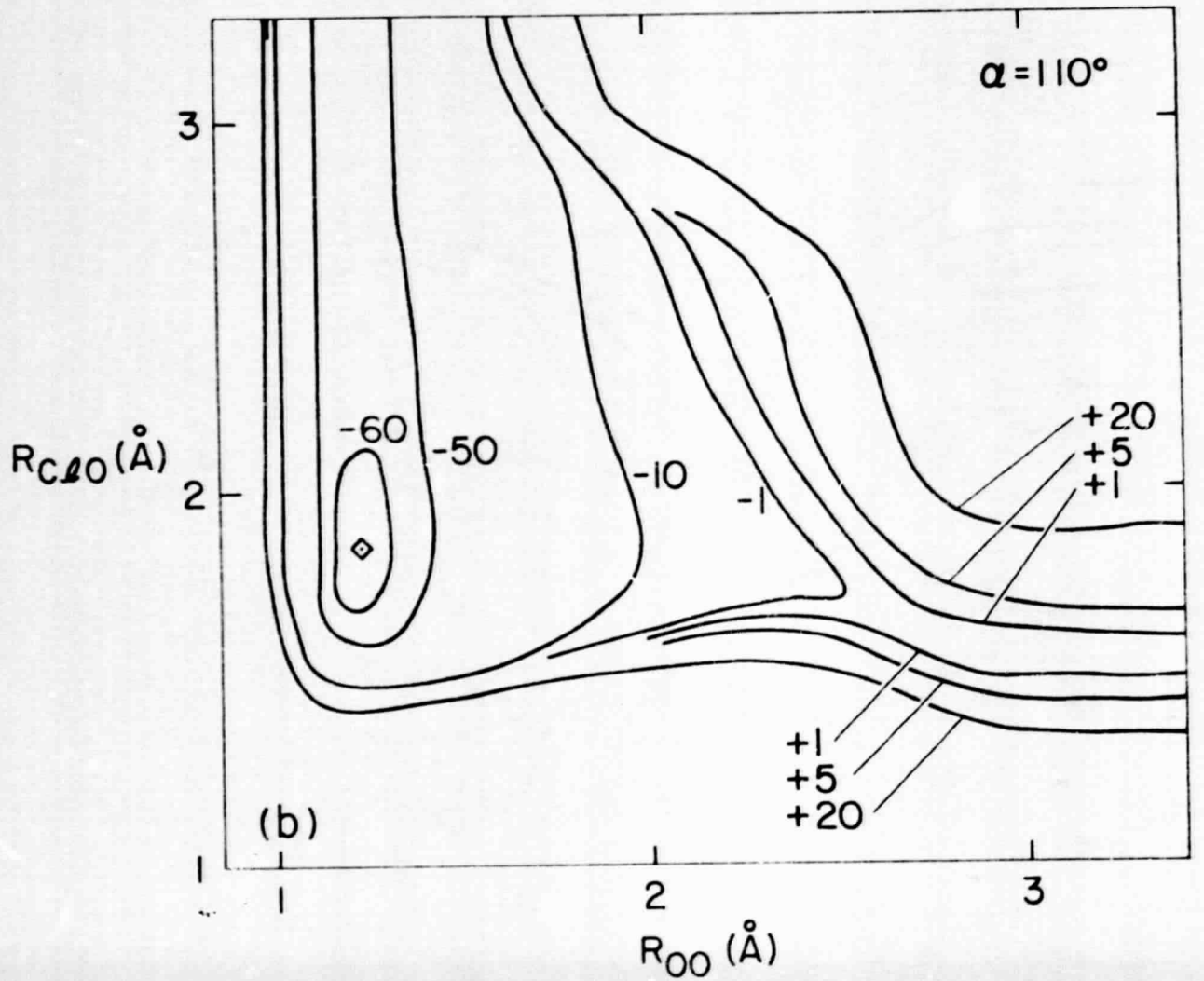


Fig. 4b

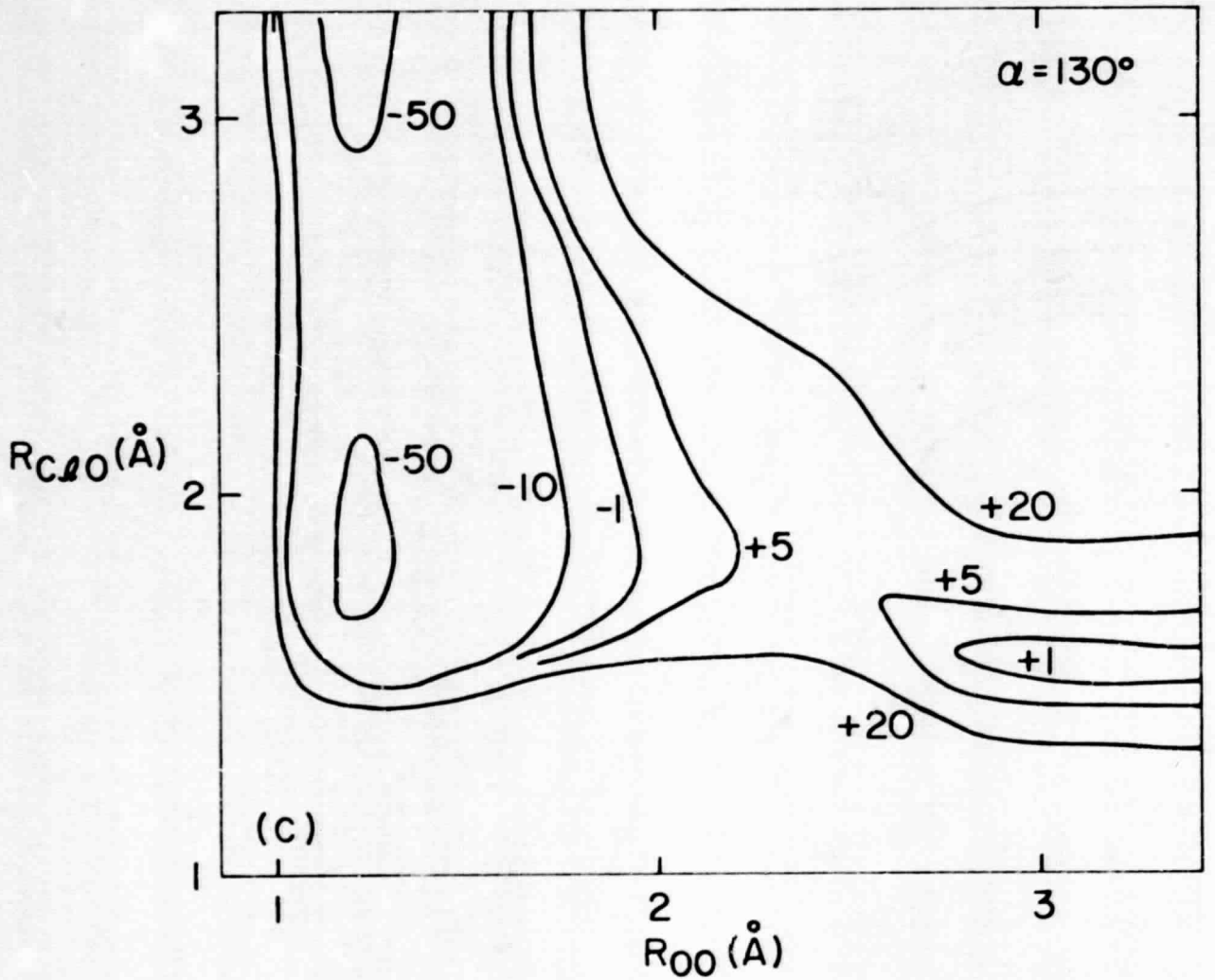


Fig. 4c

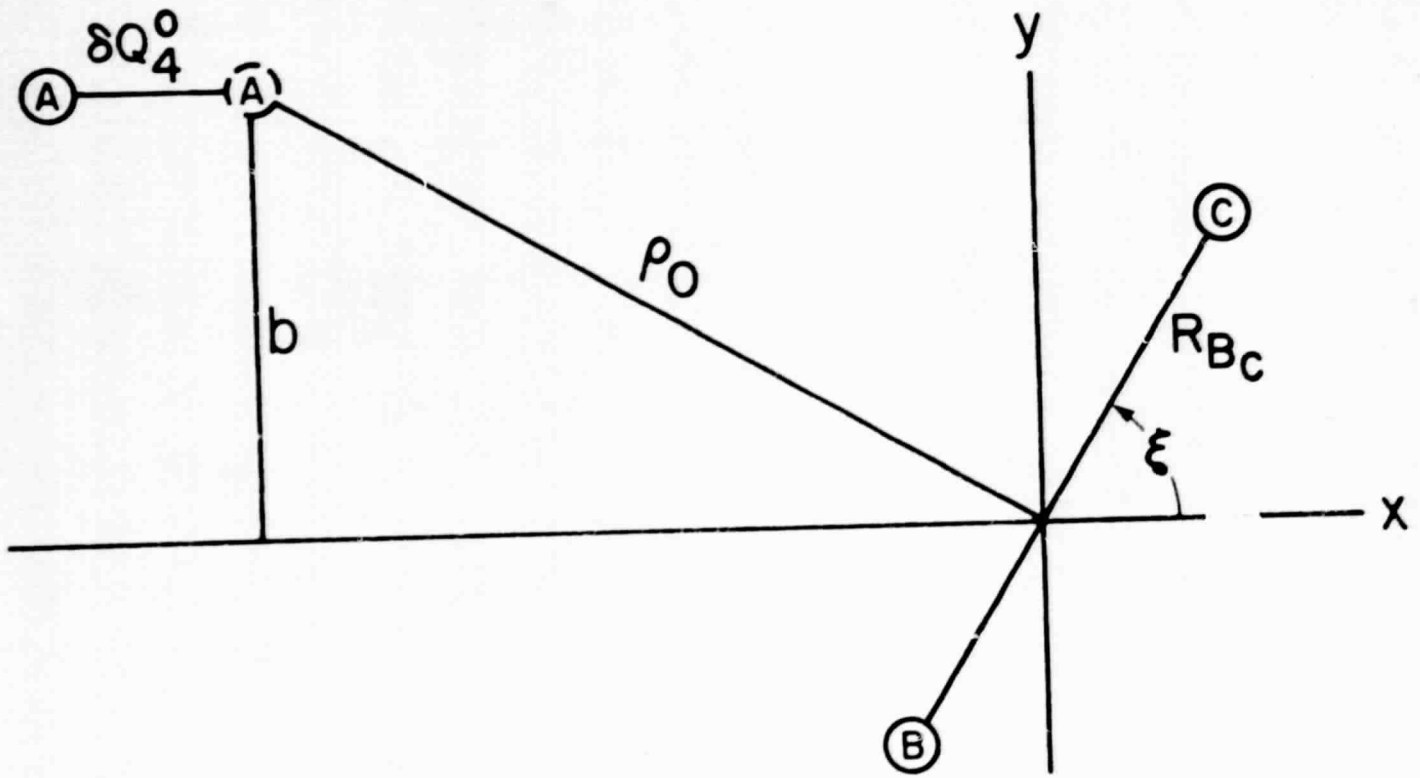


Fig. 5

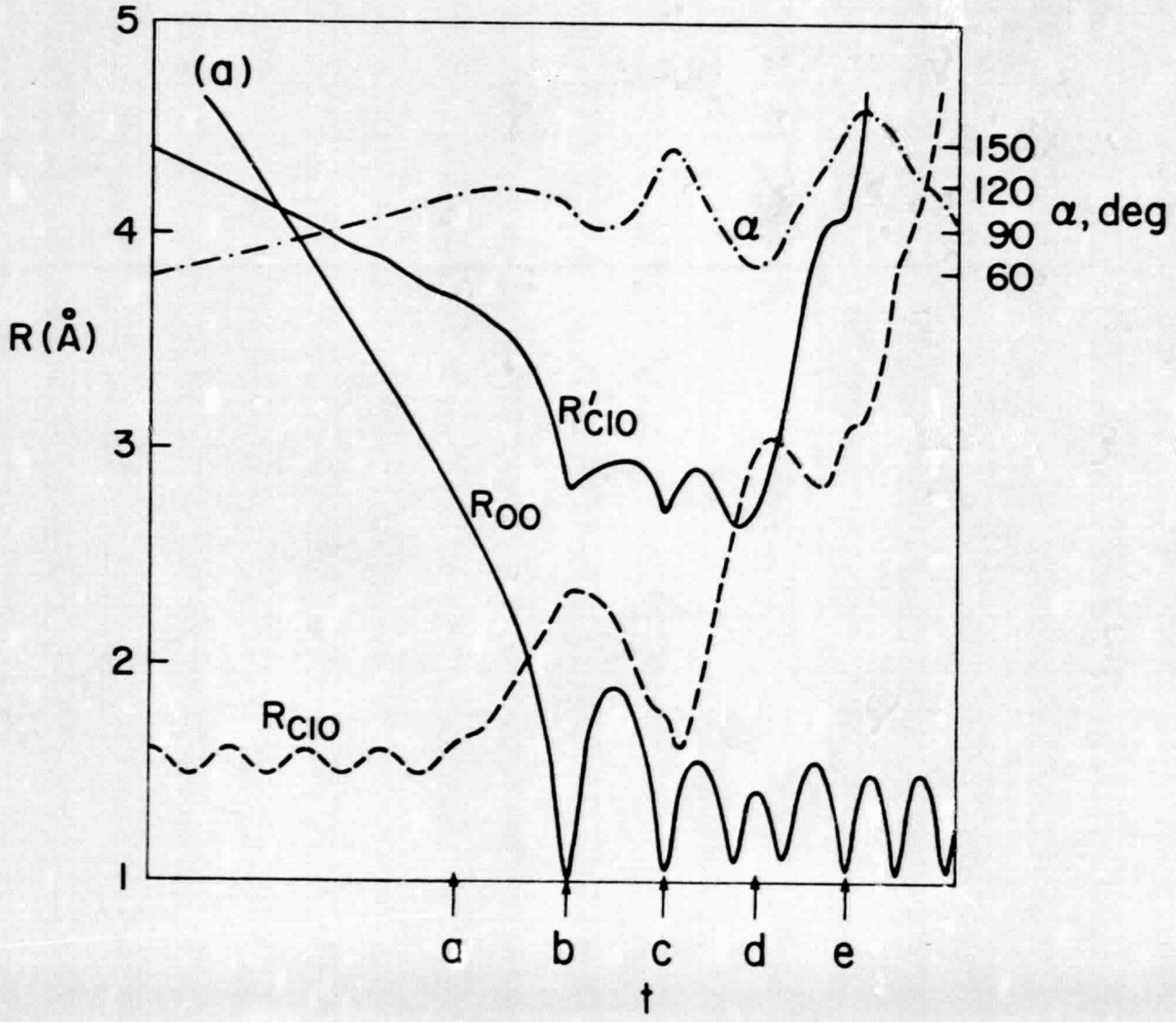


Fig. 6a

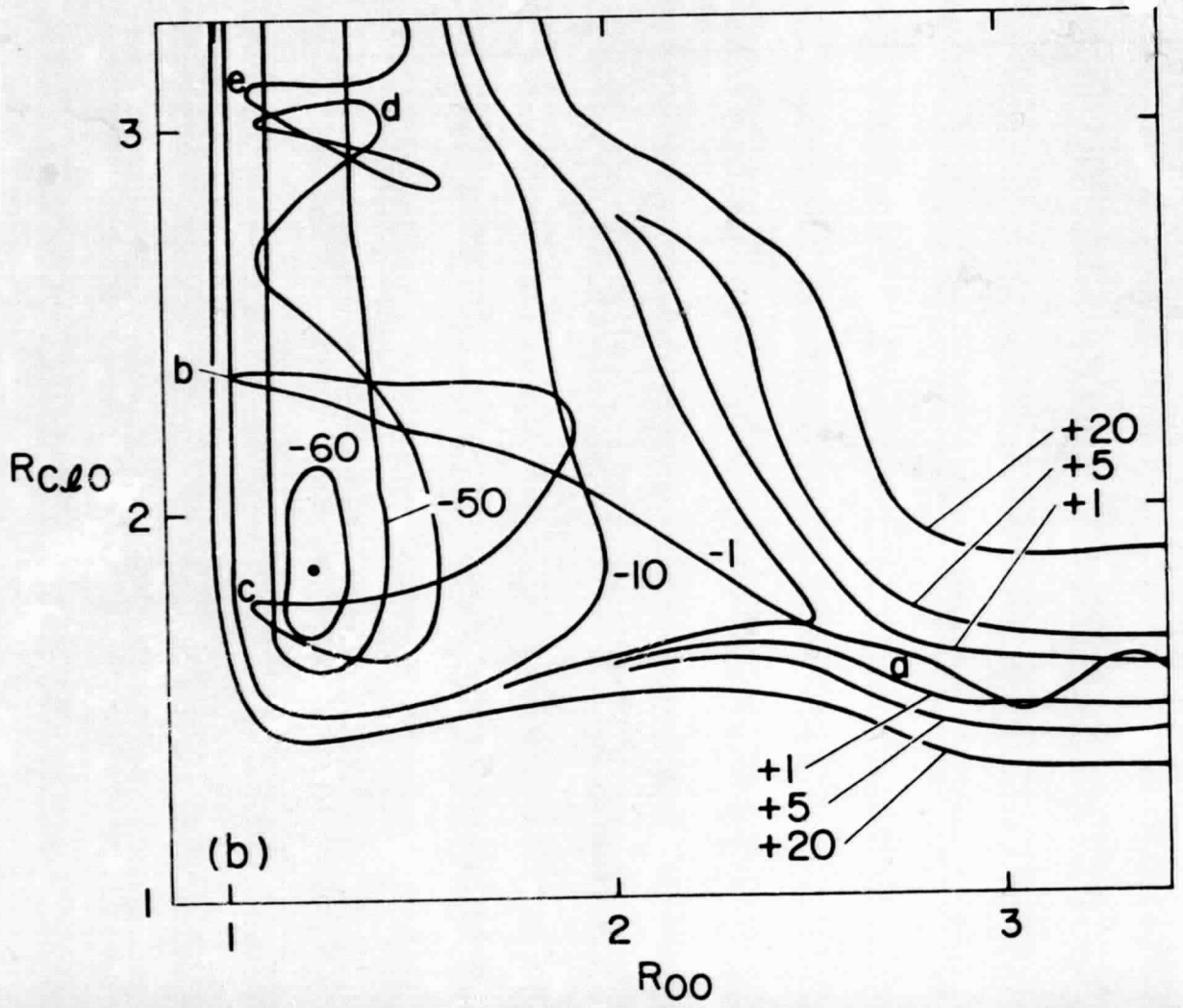


Fig. 6b

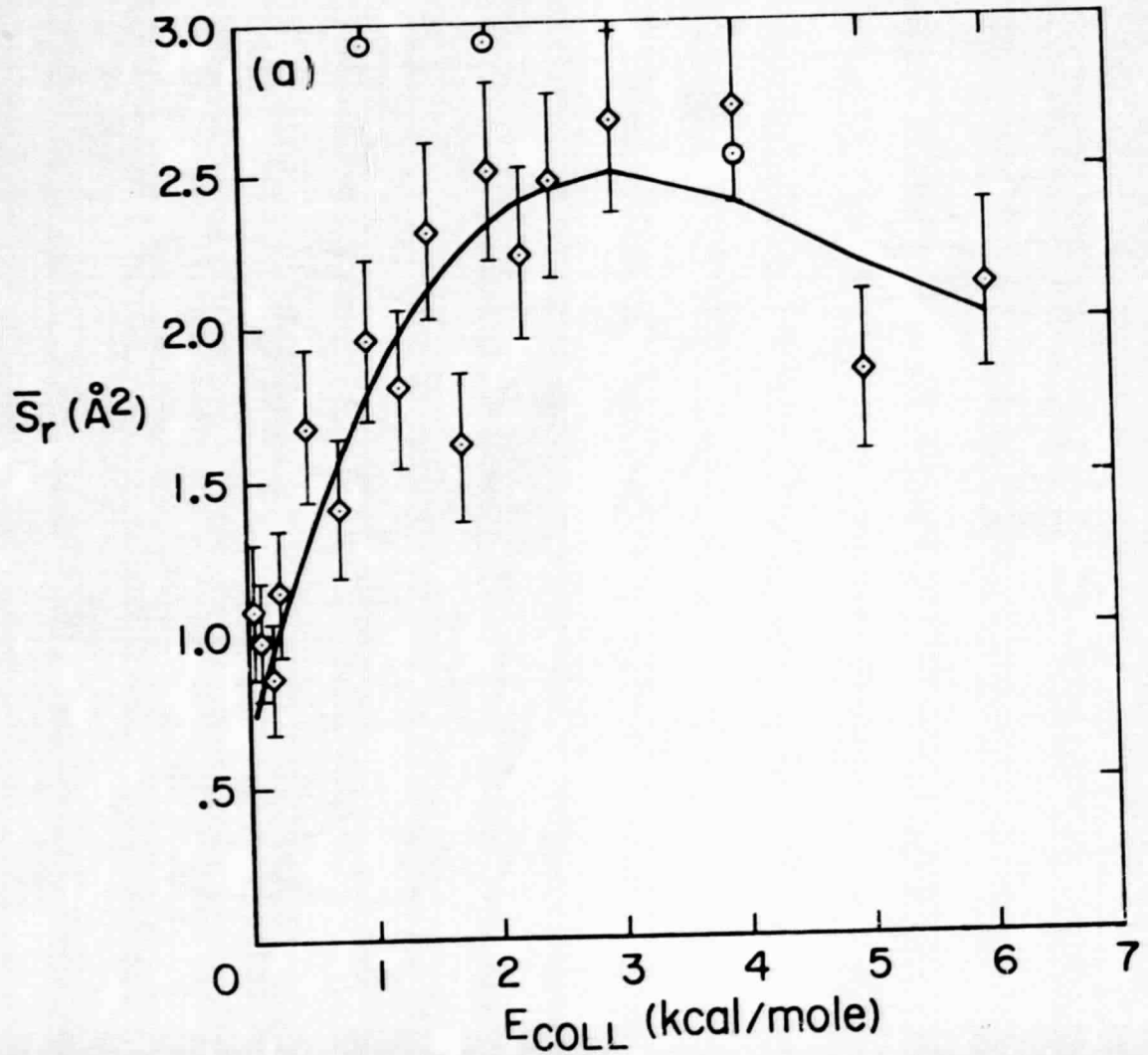


Fig. 7a

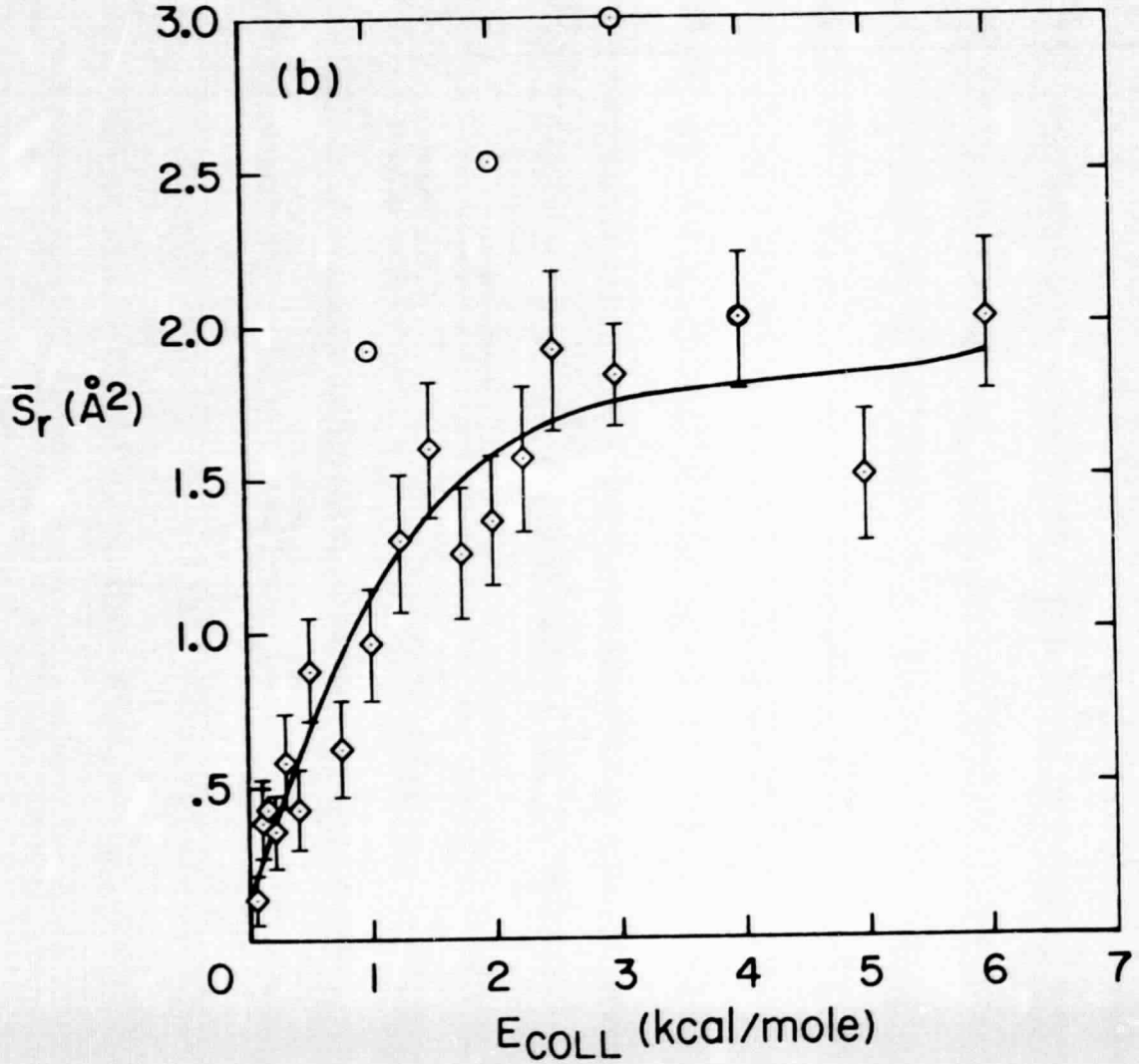


Fig. 7b

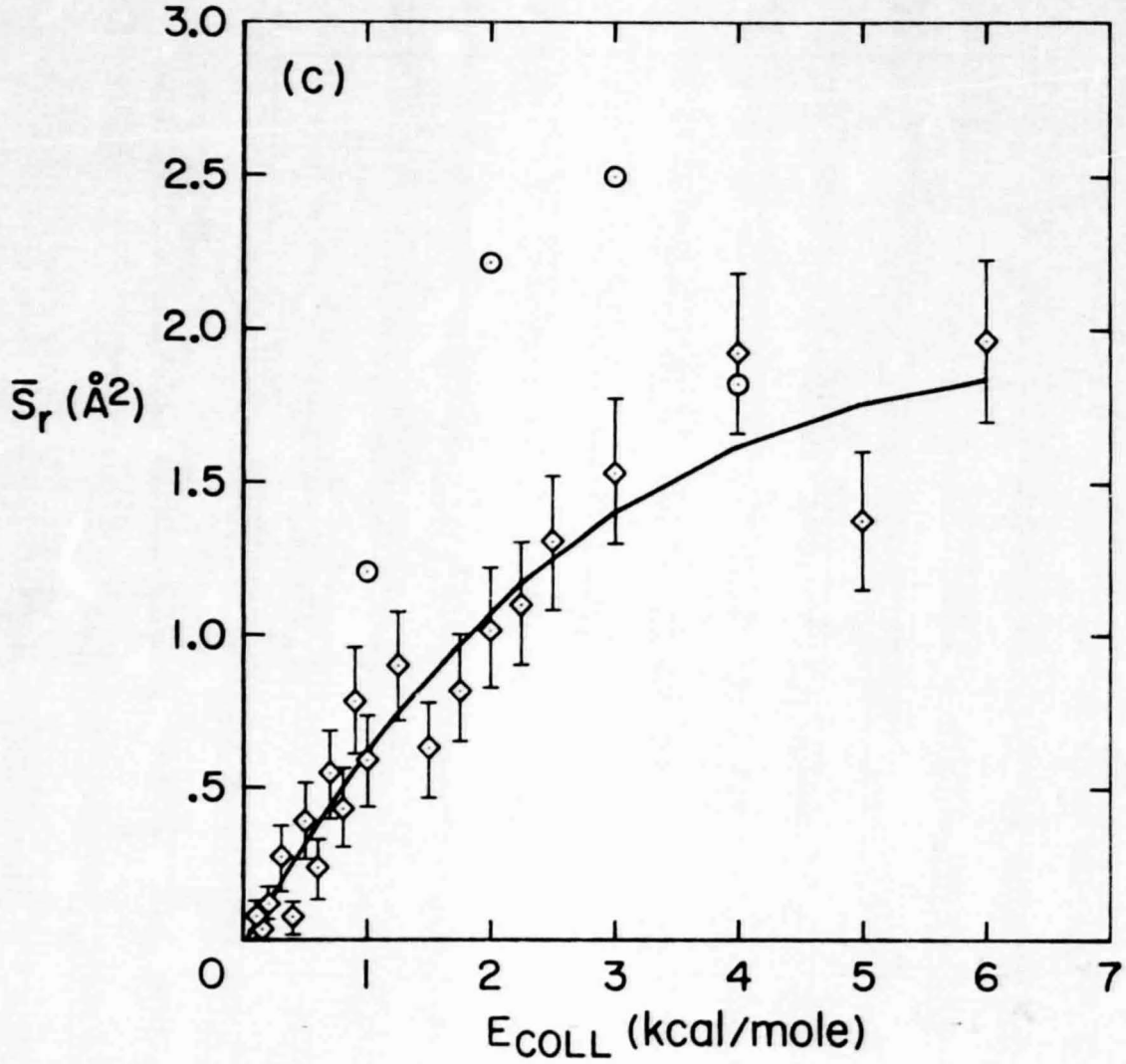


Fig. 7c

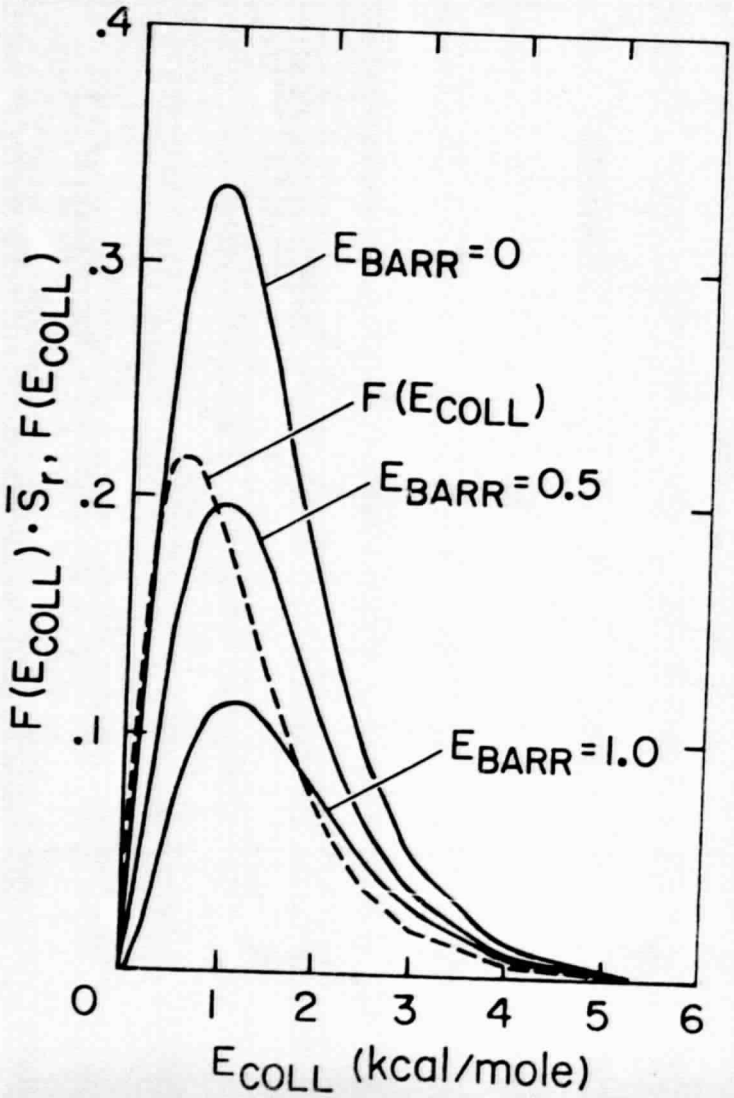
.4
.3
.2
.1
0
1
2
3
4
5
6
$E_{BARR} = 0$
$F(E_{COLL})$
$E_{BARR} = 0.5$
$E_{BARR} = 1.0$
$F(E_{COLL}) \cdot \bar{S}_r, F(E_{COLL})$
$E_{COLL}$ (kcal/mole)

Fig. 8

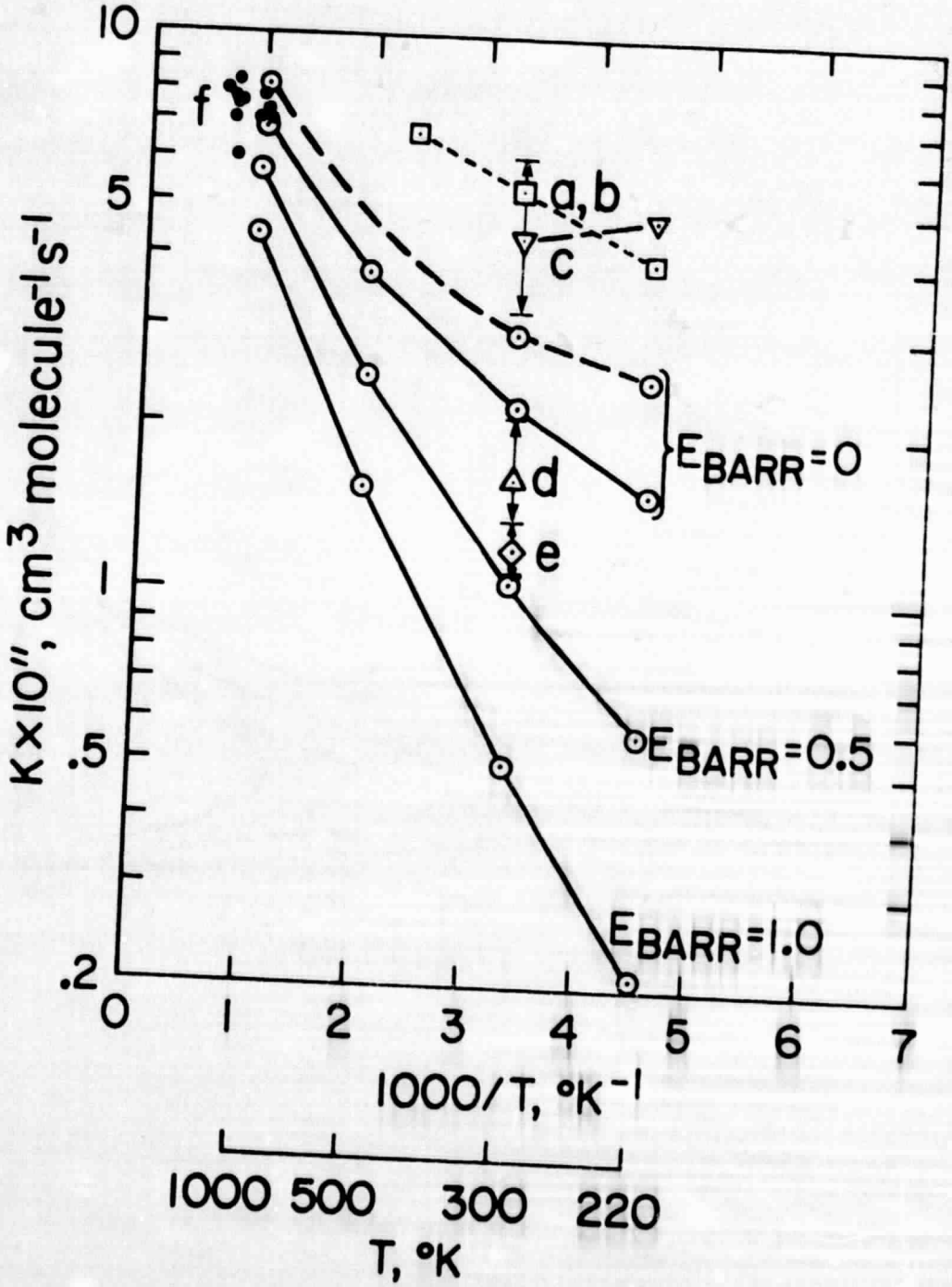
10
5
1
.5
.2
K×10'', cm³ molecule⁻¹s⁻¹
f
a,b
c
d
e
E_BARR=0
E_BARR=0.5
E_BARR=1.0
0
1
2
3
4
5
6
7
1000/T, °K⁻¹
1000 500 300 220
T, °K

Fig. 9

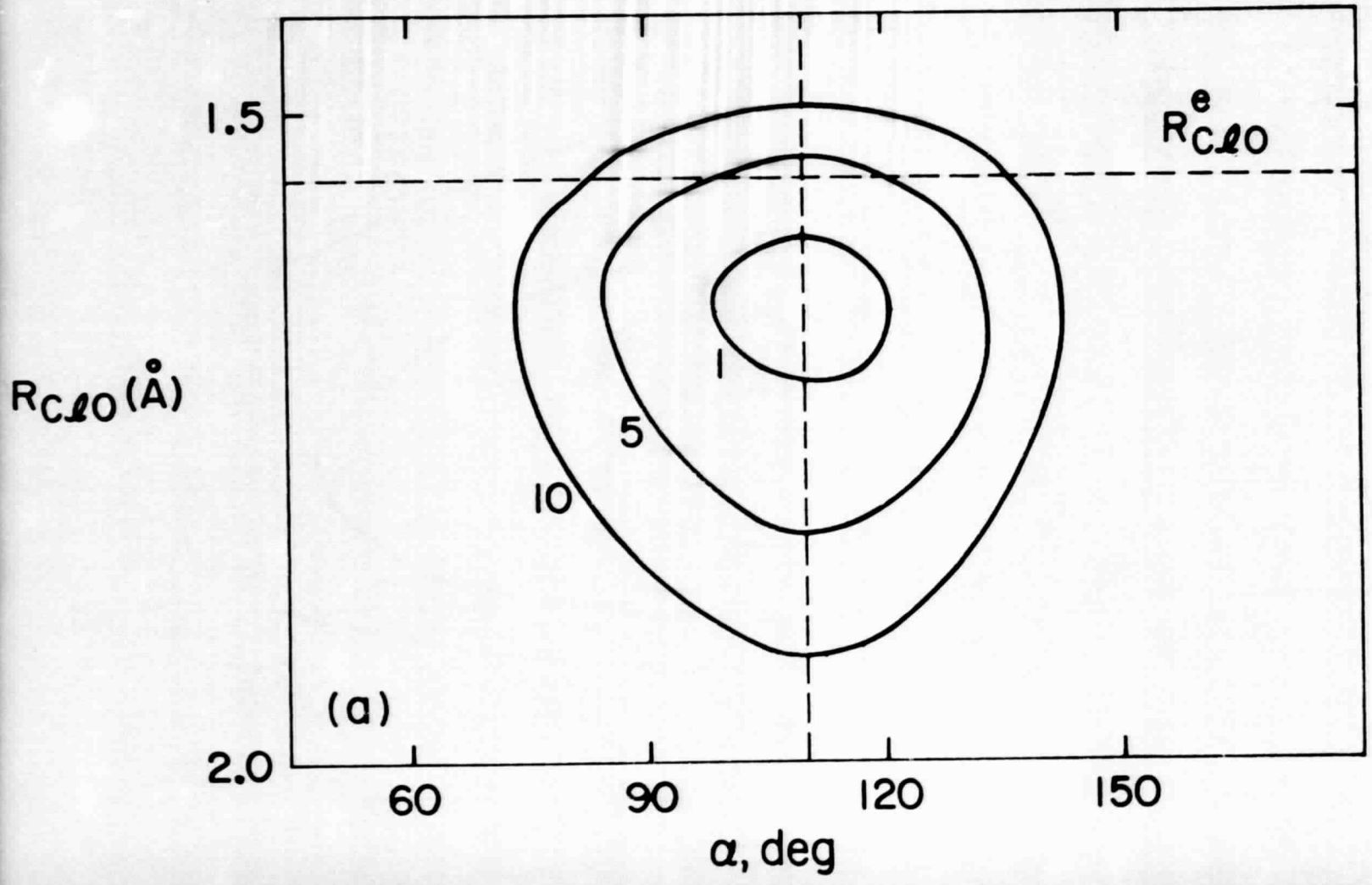


Fig. 10a

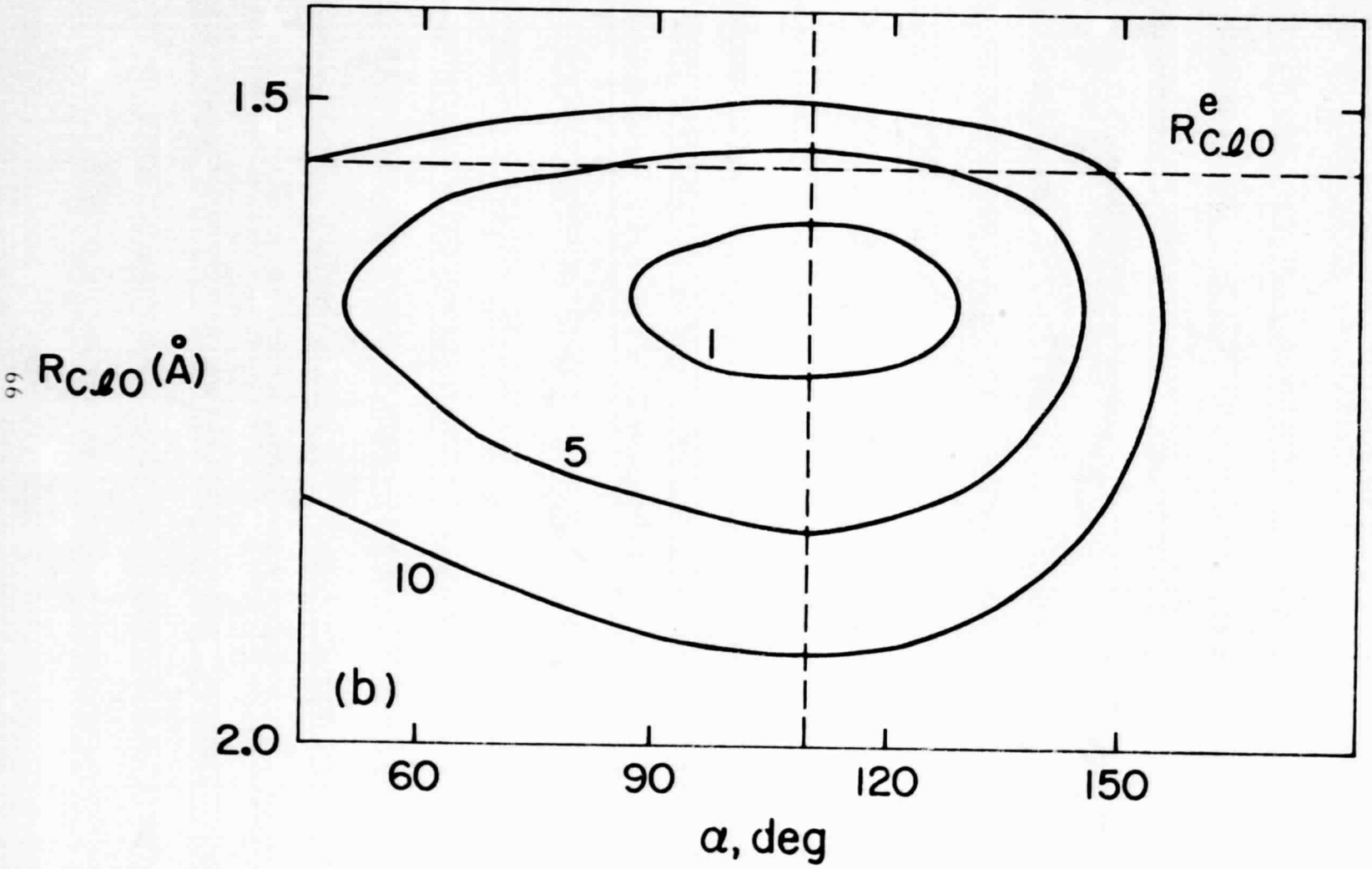


Fig. 10b

| 1. Report No. | 2. Government Accession No. | 3. Recipient's Catalog No. |
|---|---|---|
| NASA TM-78483 | | |

| 4. Title and Subtitle | 5. Report Date |
|---|---|
| CALCULATED RATE CONSTANTS FOR THE REACTION $ClO + O \rightarrow Cl + O_2$ BETWEEN 220 AND 1000 °K* | 6. Performing Organization Code |

| 7. Author(s) | 8. Performing Organization Report No. |
|---|---|
| Richard L. Jaffe** | A-6613 |
| | 10. Work Unit No. 506-16-11 |

| 9. Performing Organization Name and Address | 11. Contract or Grant No. |
|---|---|
| NASA Ames Research Center<br>Moffett Field, Calif. 94035 | |
| | 13. Type of Report and Period Covered: Technical Memorandum |

| 12. Sponsoring Agency Name and Address | 14. Sponsoring Agency Code |
|---|---|
| National Aeronautics and Space Administration<br>Washington, D. C. 20546 | |

15. Supplementary Notes

*Submitted to Journal of Chemical Physics.
**National Research Council Associate.

16. Abstract

The results of classical trajectory calculations are presented for the reaction $ClO + O \rightarrow Cl + O_2$. This reaction is an important step in the chlorine-catalyzed destruction of ozone which is thought to occur in the stratosphere. Rate constants have been calculated for temperatures between 220 and 1000 °K. The calculated rate constant is $4.36 \times 10^{-11} \exp(-191/T)$ $cm^3$ $molecule^{-1}$ $s^{-1}$ and its value at 300 °K is $2.3 \pm 10^{11}$ $cm^3$ $molecule^{-1}$ $s^{-1}$, about a factor of 2 lower than the recent experimental measurements. The calculated activation energy of 0.38 kcal/mole is in excellent agreement with the experimental value of 0.44 kcal/mole determined by Clyne and Nip and provides support for their measurements. The calculations were performed using both the quasi-classical and phase space trajectory sampling methods. The empirical potential energy surface used in the calculations was constructed to fit experimental data for ClO, $O_2$ and ClOO molecules. Other important features of this potential surface, such as the barrier to reaction, were varied systematically and calculations were performed for a range of conditions to determine the "best" theoretical rate constants. The present results demonstrate the utility of classical trajectory methods for determining activation energies and other kinetic data for important atmospheric reactions.

| 17. Key Words (Suggested by Author(s)) | 18. Distribution Statement |
|---|---|
| Rate constants<br>Activation energy<br>Classical trajectory calculation | Unlimited<br>STAR Category - 23 |

| 19. Security Classif. (of this report) | 20. Security Classif. (of this page) | 21. No. of Pages | 22. Price* |
|---|---|---|---|
| Unclassified | Unclassified | 66 | $4.50 |

*For sale by the National Technical Information Service, Springfield, Virginia 22161